Abstract

Opticruise is an automated transmission system for manual gear boxes. The length stroke is a part of the Opticruise system, in which the mechanical gear shifting process is performed by pneumatic actuators. To reduce piston velocity before the cylinder walls are reached, an oil damper is attached to the pneumatic actuator. The purpose of this thesis is to evaluate if the oil damper can be replaced by a pneumatic feedback control law, a model predictive control scheme or an alternative mechanical construction; in the interest of cost reduction, robustness, shift comfort and shift time.

To be able to do a systematic analysis, a mathematical model of the length stroke is developed. The model, developed using a length stroke that is not mounted on a truck, captures the essential dynamics of the system and is used to evaluate control strategies and investigate system properties.

As the delay in feedback information from the different sensors is larger than the process time constant, a pneumatic feedback control law is discarded. A model predictive control law is found difficult to realize since the system properties, when the length stroke is placed on a truck, are different in every gearshift. Instead a mechanical construction proposing smaller final chamber volumes is discussed. This solution turns out to be a cost-effective way to achieve a good velocity reduction before the end position.

Since feedback control is still an interesting option for future gear shifting systems, the requirements on sensors, controllers and actuators for achieving good controller performance is briefly discussed.

Contents

Chapter 1

Introduction

This master thesis project is performed at Scania CV AB, for the departments of Powertrain control systems and Mechanical maneuvering, in collaboration with the Automatic control group at KTH, School of Electrical Engineering. Scania's main focus is on heavy duty trucks and diesel engines for industrial and marine applications.

Opticruise is an automated manual transmission system found in many of Scania's recently produced heavy duty trucks. It basically consists of pneumatic force actuators for the actual gear shifting and a control unit handling the clutching work. Opticruise handles the side stroke and the length stroke, both which have three positions. The length stroke has forward, neutral and backward positions while the side stroke has right, control and left positions. These names do not have anything to do with the truck movement, they only refer to how the gears are shifted inside the gearbox.

In this paper only the length stroke part of the Opticruise system is considered.

1.1 Background

In the interest of cost reduction every part is considered. To reduce component wear due to the strong forces involved in the gear shifting, an oil damper is mounted on the length stroke. If the oil damper can be replaced by pneumatic feedback control the amount of components can be reduced.

1.2 Thesis objectives

The main thesis objective is to model a lab setup of the length stroke and preferably replace the oil damper with a pneumatic feedback control law. If this is not possible alternative ideas for replacement of the oil damper shall be considered. Apart from the oil damper, cost reduction and improvements in robustness, shift comfort and shift time concerning the length stroke in general is encouraged.

1.3 Notation

Parameter	Description
Pneumatic force actuator	
$F_{friction}$	friction force acting on the stay and piston
P_1	pressure in chamber one
P_2	pressure in chamber two
A_1	effective piston area in chamber one
A_2	effective piston area in chamber two
V_1	volume in chamber one
V_2	volume in chamber two
R_{air}	gas constant
$\dot{m}_{air}$	massflow of air
q_{in}	heat transfer term
q_{out}	heat transfer term
γ	specific heat ratio
C_v	specific heat at constant volume
T_{in}	incoming air flow temperature
α	heat transfer coefficient
α_m	heat transfer coefficient
D_{rise}	valve open time delay
D_{fall}	valve close time delay
P^*	critical pressure
$P_{stagnation}$	stagnation pressure for air
C_d	valve discharge coefficient
P_s	supply pressure
P_c	chamber pressure
A_{valve}	valve area
T_s	supply air temperature
ρ_{valve}	air density in the valve
ρ_s	supply air density
v_{valve}	air velocity in the valve
M_{air}	valve exit mach number
a_{valve}	speed of sound at valve exit
$V_{B,f}$	volume V_B when the gear is in backward
$V_{verification}$	volume for verification of mass flows
ϵ	flow of mass and temperature

Parameter	Description
Pneumatic force actuator (cont'd)	
F_{sf}	static friction
F_{df}	dynamic friction
F_{rf}	offset of dynamic friction
β	slope of dynamic friction
$F_{pressure}$	force due to pressure differences across chambers
Oil damper	
F_{oil}	counteracting force from the oil damper
$P_{oil,1}$	pressure in oil chamber one
$P_{oil,2}$	pressure in oil chamber two
A_{oil}	effective area of the piston in the oil chamber
$A_{valve,S}$	small valve area
ΔP_{oil}	pressure difference over the oil chambers
$A_{valve,B,0}$	large valve area
A_{bolt}	bolt hole area
C_d	valve discharge coefficient
q	flow of oil
κ	fluid bulk modulus
Model overwiev	
$V_{1,0}$	initial volume, chamber one
$V_{2,0}$	initial volume, chamber two
V_B	volume in chamber B
V_N	volume in chamber N
$V_{B,0}$	initial volume, chamber B
$V_{N,0}$	initial volume, chamber N
P_B	pressure in chamber B
P_N	pressure in chamber N
v	piston velocity
x_1	piston position
x_2	piston velocity
x_3	pressure in chamber one
x_4	pressure in chamber two
u_1	valve control signal, chamber one
u_2	valve control signal, chamber two
Common	
m_s	stay mass
m_p	piston mass
A_{stay}	effective stay area
x	piston position
P_{atm}	atmospheric pressure
T	temperature

Parameter	Description
Common (cont'd)	
ρ	gas/oil density
P	pressure
U	internal energy
V	volume
m	mass
$\dot{m}$	mass flow
ω_1	engine angular velocity
ω_2	driveline angular velocity
r	original piston radius

Abbreviation	Meaning
OPC4	Opticruise control unit
PWM	Pulse Width Modulation
MSE	Mean Square Error
PMP	Pontryagin's Minimum Principle
FRO	Full Range Output
RPM	Revolutions Per Minute

Chapter 2

Opticruise

Opticruise is an automated transmission system for manual gear boxes, where the shift stick is replaced by pneumatic actuators creating a computer controlled gear shifting system. The idea is that the system itself shall choose the right gear in every situation, according to some predetermined conditions. The Opticruise gear shifting system consists of two major parts. The first part is the mechanics and control technique required to switch gear, i.e. the work previously done by the driver using the shift stick and clutch. The second part consists of the strategies to choose the right gear at every occasion to acquire good driving comfort and low fuel consumption.

Improvements in the first part, since it is being addressed in this paper, can amend properties like faster gearshifts and comfort, but also reduce wear and damage to the driveline.

As mentioned in the introduction only the part of the Opticruise system handling the length stroke is discussed here.

2.1 Lab setup

To understand how the length stroke works it is necessary to go through the basic setup. The length stroke is shown in Figure 2.1. It consist of a pneumatic force actuator (length stroke cylinder and valve package) which produces the force required to shift gear. An oil damper which catches the system in the end of the gear shifting process and reduces wear of the components is also found. So far, since Figure 2.1 does not give away to much information of the system, it is still hard to understand how it works. Hence, a schematic picture of the length stroke is to prefer, this is found in Figure 2.2. The arrows in Figure 2.2 displays flow and force in the case of a gear shift from neutral to backward.

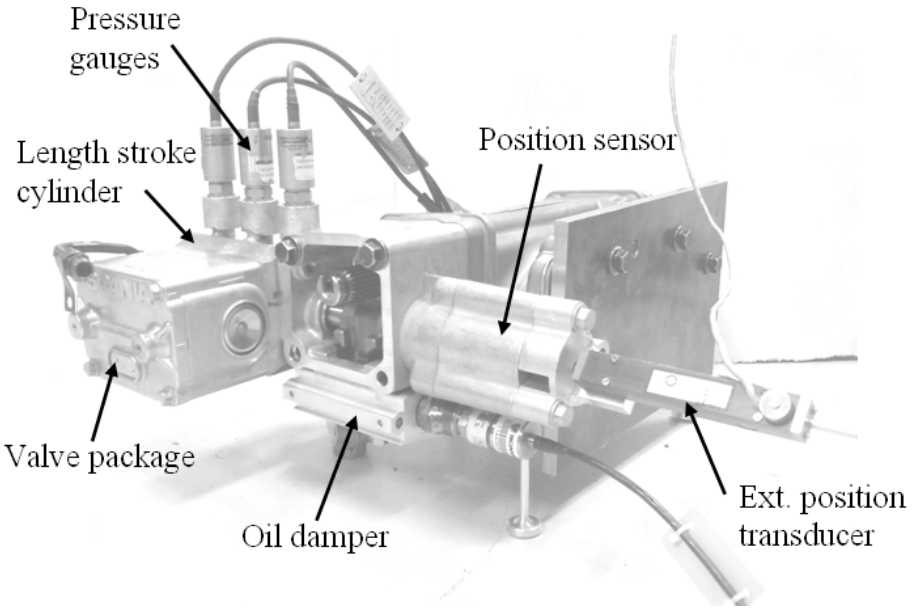

Figure 2.1. Length stroke lab setup.

2.2 Equipment

The length stroke is controlled by the OPC4 unit. To measure position an external position transducer and the built in position sensor is used. To measure pressure, pressure gauges are installed. Data acquisition is done using an oscilloscope. These are all discussed in this section.

2.2.1 OPC4

The OPC4 is the control unit handling everything concerning the length stroke, it sets the control signal and registers the position. The OPC4 is equipped with a Freescale PowerPC MPC563 CPU working at 40 MHz, 32 kByte RAM and 512 kByte flash memory, [4]. Since it handle more than the length stroke; side stroke, range, split and control strategies for gear shifting, it carries out numerous calculations in every clock cycle. Because of this, it is important to keep the code short and effective to not waste calculations, therefore the OPC4 only samples at 100 Hz, every 10 ms that is. This is slow in relation to the fast course of event when shifting gear. However, the OPC4 is not bound to sample only at 100 Hz, [4], it can sample faster if desired. As an alternative it is possible to sample only the position sensor at a faster rate, which is advantageous if feedback control is considered. However, the current code does not allow this, so new code is necessary.

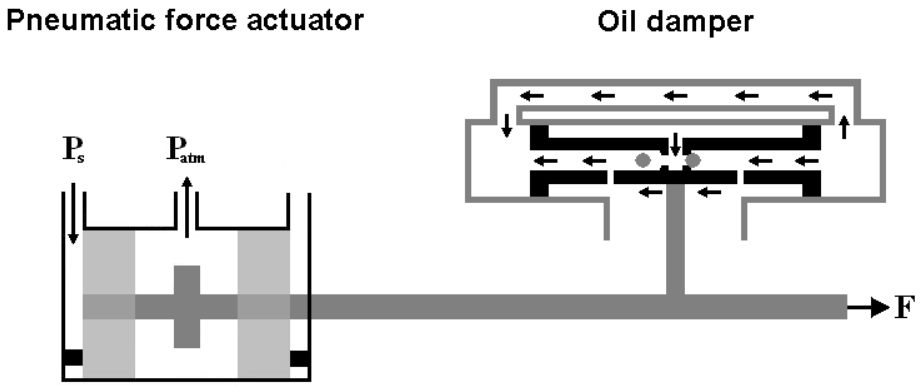

Figure 2.2. A schematic description of the length stroke.

2.2.2 Pressure gauges

To measure pressure in the pneumatic actuator and in the oil damper, Schaevitz P901 strain gauge absolute pressure transducers are used, see Figure 2.1. They are commonly used for hydraulic pressure monitoring and they have an accuracy of less than 0.10% FRO (Full Range Output), [19]. For the pneumatic actuator, pressure gauges with the pressure range 0-10 Bar are used and for the oil damper, 0-50 Bar.

2.2.3 External position transducer

The external position transducer from Swema, [22], (type: 248.105 RLP) is a linear thread wounded precision potentiometer, used to indicate and measure positions and change in positions (see Figure 2.1). The stainless steel shaft is used together with bronze bearings and rotates freely to minimize influence from moments of torsion. The maximum starting force is low, between 0.25 and 2 N and the resolution high, 0.05 mm. Due to the low starting force, friction from the sensor is neglected.

2.2.4 Length stroke position sensor

The length stroke position sensor, also referred to as the internal position sensor, is an inductive sensor consisting of a fixed coil with a movable core mounted to the stay. The inductance in the coil varies as the stay moves back and forth. The setup is better illustrated in Figure 2.3. The right hand side of Figure 2.3 shows how the sensor works in a step by step sense.

1. The micro controller inside the OPC4 sends out a pulse signal to the position sensor circuit.

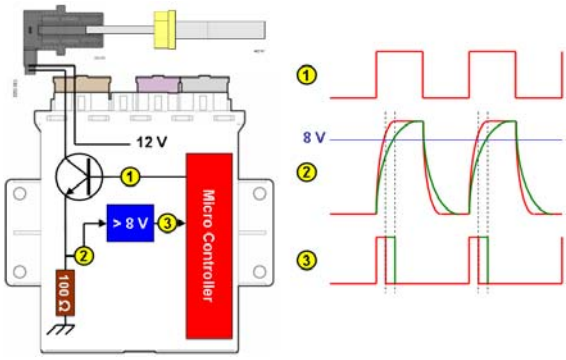

Figure 2.3. The Opticruise position sensor and OPC4 control unit.

2. The inductance in the coil varies, depending on the flange screw position in the coil. The inductance determines how long time it takes to reach 8 volt.

3. The time to reach 8 volt is converted into a pulse signal. By measuring the pulse duration and current temperature, a value corresponding to the position is obtained.

A major drawback with this sensor is that it is slow compared to the potentiometer sensor discussed earlier. As illustrated in Figure 2.4, the length stroke position

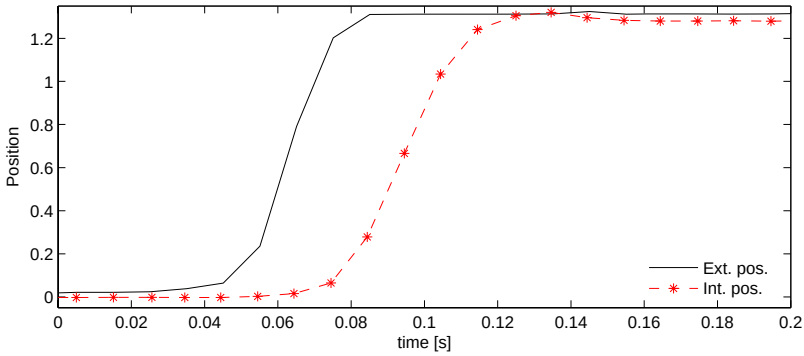

Figure 2.4. The length stroke position sensor compared to the external position transducer.

sensor is 30 ms behind in time compared to the external sensor when motion is started. In Figure 2.4 the time difference between the internal and external position sensor reaches 40 ms in the end of the piston movement. Measurements from gear shifts in the truck indicate that the sensor is even slower during longer processes.

The main reason for the sensor being slow is the OPC4 unit. In the OPC4 the signal from the sensor is filtered with a Butterworth filter, [4]. If this filter is removed, a factor three can be saved on the response time. Removing the filter makes the signal follow the one of the external sensor better and not slack as time passes. The sensor is then only limited by the sampling time on the OPC4 unit. It is previously stated that the time it takes to reach 8 volts determines the position; this time interval is about 0.9 ms, [4], (see Figure 2.5). If the sampling time on the OPC4 is reduced to fit the time needed for the inductive sensor to reach over 8 volts and discharge to 0 volts, more time can be saved. This is of course at the expense of the measurement accuracy, since disturbances are not filtered. With a position measurement updated every 2-3 ms, depending on D_e, the possibility to introduce a pneumatic feedback control law has dramatically increased.

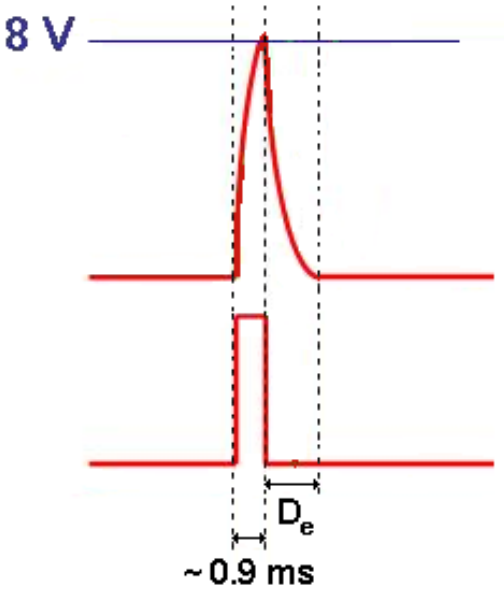

Figure 2.5. Position sensor with reduced sampling time.

2.2.5 Oscilloscope

To acquire data, a Yokogawa DL 750 digital oscilloscope is used. The oscilloscope supports sampling rates up to 2 GHz, here a sampling frequency of 10 kHz is used.

Chapter 3

The model

A gear shift in the length stroke is very similar to moving a single piston pneumatic actuator to its end position. The only difference is that in the length stroke case, the piston can move freely on the stay for a short distance. Therefore, to simplify calculations, a pneumatic actuator with a fixed piston is first considered. This model is then transformed to correspond to the length stroke. Since the length stroke and fixed piston pneumatic actuator has the same properties, the fixed piston pneumatic force actuator is used for further analysis because it is more convenient to use.

3.1 Pneumatic force actuator

Figure 3.1 describes a pneumatic force actuator system. A pressure supply with constant pressure P_s is connected through a valve to a chamber with a moving piston. On the other side of the piston there is an exhaust chamber connected only to atmospheric pressure.

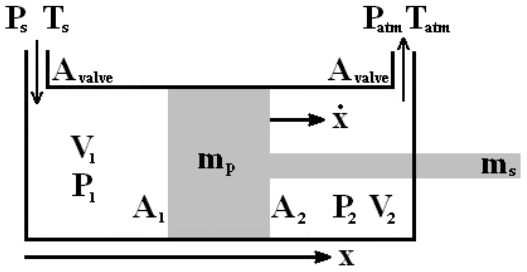

Figure 3.1. Schematic picture of a pneumatic force actuator.

The pneumatic force actuator system in Figure 3.1 can be split up into two

processes, a charging process (left chamber) and a discharging process (right chamber). Work modeling pneumatic actuators goes back to the 1950's. One of the classical papers is written by Shearer, [20], and is often credited as the ground breaking within this area.

When modeling these two processes, the general assumptions are that the processes are either isothermal (no temperature change in the system) or adiabatic (no heat exchange with the surroundings). As in this case, these processes are generally rapid and therefore often considered as adiabatic. This approach is used by Bobrow and McDonell, [3], and Kazerooni, [10], to model pneumatic actuators similar to the one presented above.

However, work by Al-Ibrahim and Otis, [1], shows that the temperature in the charging process follows the one of the adiabatic process while the isothermal process better corresponds to the discharging process. Meanwhile, Ning et al., [14], concludes that the high turbulence in the charging process should result in a high heat transfer coefficient and therefore be close to the isothermal process. The discharging process which has a lower turbulence and lower heat transfer should be closer to the adiabatic process. Richer and Hurmuzlu, [18], account for both these characteristics by creating a model that stands for both the adiabatic and the isothermal case.

Here, theory presented in [18] and [3] will be used to model the system presented in Figure 3.1.

3.1.1 Piston-stay dynamics

Using [18], the equation of motion for the piston-stay setup is,

$$(m_s + m_p)\ddot{x} - F_{friction}(\dot{x}) = P_1 A_1 - P_2 A_2 - P_{atm} A_s \tag{3.1}$$

where m_s and m_p are the mass of the stay and piston respectively. x is the piston position, $F_{friction}(\dot{x})$ is the friction force as a function of the piston velocity, P_1 and P_2 are the pressures in the chambers and A_1 and A_2 are the effective areas of the piston, all according to Figure 3.1. Furthermore, A_s is the effective area of the stay.

3.1.2 Chamber pressure dynamics

As discussed earlier, work by Al-Ibrahim and Otis, [1], indicate that the charging process, favourably, can be modeled as adiabatic and the discharging process as isothermal, while Ning et al., [14], indicate the opposite. Since both of these cases are taken into account by Richer and Hurmuzlu, [18], their work will lay ground for this model. To create a model for the chamber pressure the ideal gas law, the continuity of mass and the energy equation are necessary. One form of the ideal gas law is,

$$P = \rho R_{air} T \tag{3.2}$$

where P is the pressure, ρ is the density, R_{air} is the gas constant and T is the temperature. The mass flow is the change in mass and therefore (in accordance with the continuity of mass),

$$\dot{m} = \frac{\partial}{\partial t}(\rho V) \tag{3.3}$$

According to [18] the energy equation in a chamber, or control volume, can be written as:

$$q_{in} - q_{out} + \gamma C_v(\dot{m}_{in}T_{in} - \dot{m}_{out}T) - \dot{W} = \dot{U} \tag{3.4}$$

In (3.4) q_{in} and q_{out} are the heat transfer terms, γ is the specific heat ratio, C_v is the specific heat at constant volume, $\dot{m}_{in}$ and $\dot{m}_{out}$ are the mass flows in and out of the chamber, T_{in} is the temperature of the incoming air flow and $\dot{W}$ is the rate of work change. $\dot{U}$ is the internal energy change,

$$\dot{U} = \frac{\partial}{\partial t}(C_v m T) = \left\{ C_v = \frac{R_{air}}{\gamma - 1} \right\} = \frac{1}{\gamma - 1}\frac{\partial}{\partial t}(PV) = \frac{1}{\gamma - 1}\left(V\dot{P} + \dot{V}P\right) \tag{3.5}$$

In this case the isolation between the piston and chamber is of rubber seal type. Richer and Hurmuzlu, [18], assumes that there is no mass flow of air between the chambers during such conditions, this is also assumed here. Furthermore it is assumed that the incoming flow has the same temperature as the air in the chamber (Outgoing flow has the same temperature as in the chamber). Using this and the fact that $\dot{W} = P\dot{V}$ together with (3.5), (3.4) evolves into:

$$\frac{\gamma - 1}{\gamma}(q_{in} - q_{out}) + \frac{1}{\rho}\dot{m} - \dot{V} = \frac{V}{\gamma P}\dot{P} \tag{3.6}$$

Considering the process as adiabatic ($q_{in} - q_{out} = 0$) and using (3.2) to eliminate ρ, an expression for $\dot{P}$ is obtained,

$$\dot{P} = \gamma\frac{R_{air}T}{V}\dot{m} - \gamma\frac{P}{V}\dot{V} \tag{3.7}$$

If the process is instead assumed to be isothermal (constant temperature) the internal energy change is:

$$\dot{U} = C_v\dot{m}T \tag{3.8}$$

With this expression for the internal energy, the resulting isothermal energy equation is,

$$q_{in} - q_{out} = P\dot{V} - \frac{P}{\rho}\dot{m} \tag{3.9}$$

eliminating ρ with (3.2) and solving for $\dot{P}$ results in:

$$\dot{P} = \frac{R_{air}T}{V}\dot{m} - \frac{P}{V}\dot{V} \tag{3.10}$$

The only difference between (3.7) and (3.10) is the specific heat ratio term γ. Therefore both equations can be combined into one, as in [18], using the notations α_m and α:

$$\dot{P} = \underbrace{\alpha_m \frac{R_{air}T}{V}\dot{m}}_{\text{change in } P \text{ due to massflow}} - \underbrace{\alpha\frac{P}{V}\dot{V}}_{\text{change in } P \text{ due to volume change}} \tag{3.11}$$

The coefficients α_m and α depend on the heat transfer during the process, these are unknown but in theory found between 1 and γ depending on the nature of the process (isothermal or adiabatic). However, as hinted in [1], α_m should be closer to γ if it is a charging process and closer to 1 if it is a discharging process and the same goes for α.

3.1.3 Valve

The three valves in the length stroke pneumatic force actuator are of on/off solenoid type. The valves consists of a copper coil, within the coil a spring mounted steal plunger is situated. Applied voltage forces the steal plunger to move, opening the valve. When the voltage is removed the spring forces the plunger to close the valve.

Work, modeling solenoid actuators is carried out by Topcu et al., [24], Song-Min et al., [21], and Rahman et al., [16]. They all use pulse width modulation (PWM) to achieve a linear relationship between flow and valve voltage. However, while Topcu et al., [24], produce a detailed physical model of the solenoid valve, Song-Min et al., [21], and Rahman et al., [16], experimentally determines the non-linear relationship of flux linkage against current and plunger position. To produce these kinds of models the coil current, flux linkage and plunger position must be measured. The equipment available and the solenoid valves in the valve package do not allow such measurements.

The solenoid valves in the valve package are used with a PWM with 98 percent duty cycle. Experiments are carried out to determine whether the flow can be controlled if the duty cycle is changed, so called pulsing. The result shows that for a duty cycle of 33 percent the valve is closed, and for 35 percent it is open, leaving no room for control. The valves are therefore modeled as time delays and the time delay is the time it takes after the open/close signal is distributed until the valve actually opens/closes. Furthermore, the complex nature of the valve characteristics are modeled as effects on the mass flow and therefore discussed in 3.1.4.

Figure 3.2 shows the pressure in chamber one and the valve control signal. The time difference between high/low in control signal and when the pressure starts to rise/fall is the response time of the valve and thus the time delay is obtained. The time delay, D_{rise}, is measured to 8 ms and D_{fall} to 35 ms. Håkansson and Johansson, [6], use similar valves, but flow controllable. They mention that the valve's closing and opening times are very sensitive to temperature and pressure changes. The result should be considered with this in mind.

The valves are relatively fast to open, but much slower when it comes to closing. As the solenoid valve is a magnetic load, it has to be equipped with a transient protection, a free wheel diode. This diode eliminates voltage peaks when the load is removed, but is also the explanation for the long closing time. Another way to

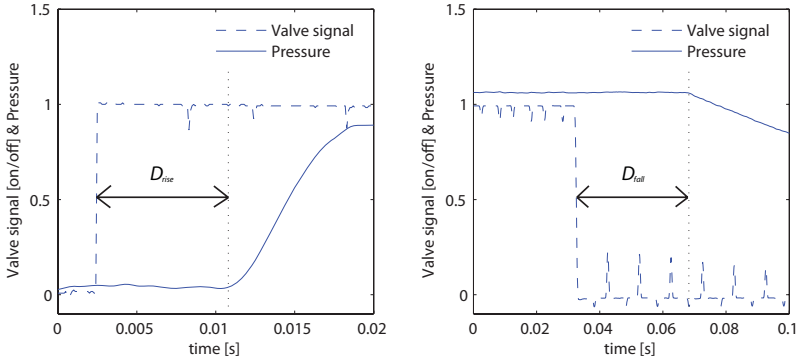

Figure 3.2. Valve open and close delays.

speed up the valve's closing time is to shorten the duty cycle on the valve. As only a duty cycle of 35 percent is required to open the valve and to keep it open, it is not necessary to apply voltage during 98 percent of the PWM signal.

3.1.4 Mass flow

As seen in 3.1 the chamber pressure depends on the mass flow through the valve. The mass flow can either be choked or free. The mass flow is choked if the ratio between the pressure inside the chamber and the pressure on the other side of the valve, P_c/P_s, is less than the ratio between the critical pressure, P^*, and the stagnation pressure for air, $P_{stagnation}$. This ratio is calculated with the isentropic flow relation according to [9] as:

$$\frac{P^*}{P_{stagnation}} = \left(\frac{\gamma+1}{2}\right)^{-\gamma/(\gamma-1)} = 0.5283 \tag{3.12}$$

Here, the reservoir pressure, P_s is equal to the stagnation pressure, $P_{stagnation}$ and the ratio P_c/P_s determines whether the flow is choked or not. In the case of a choked mass flow, i.e $P_c/P_s < 0.5283$, the mass flow is calculated according to [9] with the modifications (the discharge coefficient) taken from [14] as:

$$\dot{m}_{air} = P_s C_d \left\{ \frac{\gamma}{R_{air} T_s} \left(\frac{2}{\gamma+1}\right)^{(\gamma+1)/(\gamma-1)} \right\}^{1/2} A_{valve} \tag{3.13}$$

A_{valve} is the smallest valve area and C_d is the discharge coefficient used to model the valve characteristics. In the case of a non choked flow, it follows from [9] that the mass flow is given by,

$$\dot{m}_{air} = \rho_{valve} v_{valve} A_{valve} C_d = \rho_s \frac{\rho_{valve}}{\rho_s} M_{valve} a_{valve} A_{valve} C_d \tag{3.14}$$

where ρ_{valve} and ρ_s are the densities of air in the valve and in the reservoir, M_{valve} is the exit mach number and a_{valve} is the speed of sound at the exit. From the isentropic flow pressure ratio, according to [9], the exit mach number can be calculated as:

$$M_{valve} = \sqrt{\frac{2}{\gamma - 1}\left\{\left(\frac{P_s}{P_c}\right)^{(\gamma-1)/\gamma} - 1\right\}} \tag{3.15}$$

Moreover, $\rho_s = m_{air}/V_s$ is given by the ideal gas law, (3.2),

$$\rho_s = \frac{P_s}{R_{air}T_s} \tag{3.16}$$

and ρ_{valve}/ρ_s is calculated from the isentropic flow density relation, from [9], as:

$$\frac{\rho_{valve}}{\rho_s} = \left\{1 + \frac{\gamma - 1}{2}M_{valve}^2\right\}^{-1/(\gamma-1)} \tag{3.17}$$

a_{valve}, the speed of sound at the exit, is calculated from temperature. The temperature at the exit, T_{valve} is given by the isentropic flow temperature ratio;

$$T_{valve} = \left\{1 + \frac{\gamma - 1}{2}M_{valve}^2\right\}^{-1} T_s \tag{3.18}$$

and hereby a_{valve} is obtained, according to [9], as:

$$a_{valve} = \sqrt{\gamma R_{air} T_{valve}} \tag{3.19}$$

By joining (3.14), (3.15), (3.16), (3.17) and (3.19), the non choked mass flow is obtained,

$$\dot{m}_{air} = \frac{A_{valve}C_d P_s}{T_s}\sqrt{\frac{2\gamma T_{valve}}{(\gamma - 1)R_{air}}\left\{\left(\frac{P_s}{P_c}\right)^{(\gamma-1)/\gamma} - 1\right\}}\left\{1 + \frac{\gamma - 1}{2}M_{valve}^2\right\}^{-1/(\gamma-1)} \tag{3.20}$$

To test the accuracy of the calculated mass flow a fixed volume, $V_{B,f}$ (the volume V_B when the gear is in backward, see right picture in Figure 3.14), is filled and emptied with air experimentally and theoretically (Figure 3.3). Instead of measuring the mass flow directly, the flow of mass and temperature, according to (3.22), flowing into/out of the system is measured as a function of pressure. Figure 3.3 shows that the theoretical mass flows are poor estimations of the real mass flows, even with the discharge coefficients which tries to take into account the specific characteristics of these valves. Since it is necessary to measure the flow of mass and temperature to determine the discharge coefficient, it might be simpler to do a mapping of the mass and temperature flow. The reason for differences between the measured and theoretical flow of mass and temperature is probably a cause of the complicated pathway air takes through the valve package in the length stroke,

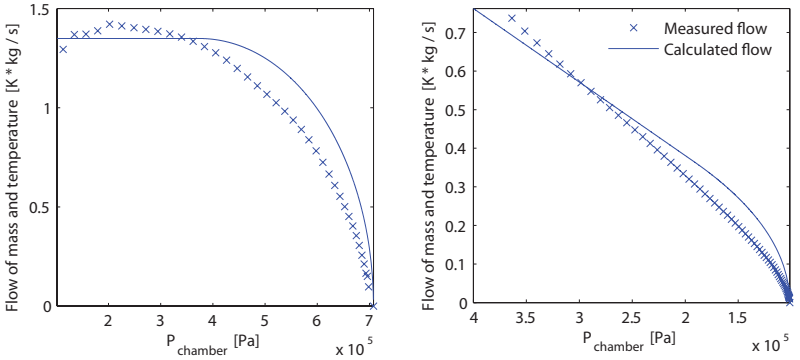

Figure 3.3. Measured flow of mass and temperature compared to theoretical. The left figure shows the charging process and the right figure shows the discharging process.

but is also believed to depend on a pressure drop in the hose between the supply and the valve in the charging process.

Similar problems are discussed in both [3] and [18]. Richer and Hurmuzlu, [18], carry out calculations to characterize the hose and valve. This is however not possible in this case due to the complex nature of the valve and the lack of information about the air pressure supply. Bobrow and McDonell, [3], proposes that the internal energy of mass flow as a function of the chamber pressure should be obtained through curve fitting. Here a method similar to the one proposed by Bobrow and McDonell, [3], is used.

The same fixed volume used previously, $V_{B,f}$, is filled and emptied with air while pressure is measured; the pressure is differentiated with respect to time and plotted aginst pressure. Hence, it is possible to calculate the flow of mass and temperature. Note that it is not necessary to measure the temperature since it is included in the flow of mass and temperature.

Two polynomial curves of different orders are fitted to the measured data (one measurement), as functions of pressure; one for the first part of the charging process and one for the second, corresponding to the high and low regions of flow as shown in Figure 3.4. Polynomials giving the least mean square error (MSE) are chosen. Since computer power is adequate the polynomials giving the lowest MSE are chosen regardless of the degree. The chosen polynomials are together convergent for the hole span of pressures used, i.e P_s to P_{atm}. For the discharging case, fitting is made in the same way.

To verify the accuracy of the polynomials and theoretical formulas describing the mass flow, tests where carried out filling and emptying a volume, $V_{verification}$, of roughly three times the size of the one used to create the polynomials. In Figure 3.5 chamber pressures are recorded and compared to the simulated chamber pressures calculated from the flow of mass and temperature polynomials and the theoretical mass flow formulas. It is concluded that the flows of mass and temperature are better estimates than the theoretical mass flows calculated earlier.
As observed in Figure 3.4 the flow of mass and temperature does not depend

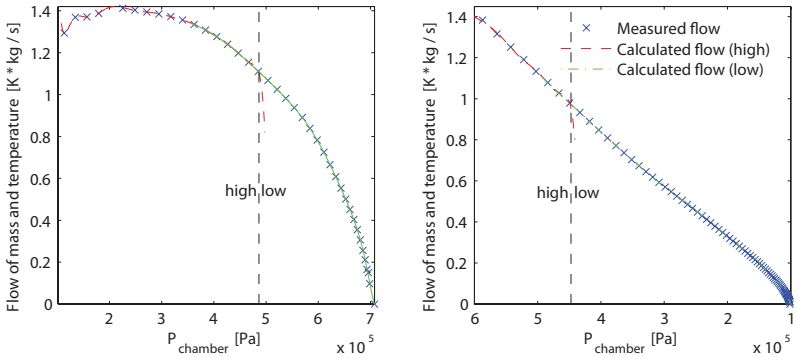

Figure 3.4. Measured flow of mass and temperature (crossed) and fitted (filled). The left figure shows the charging process and the right figure shows the discharging process.

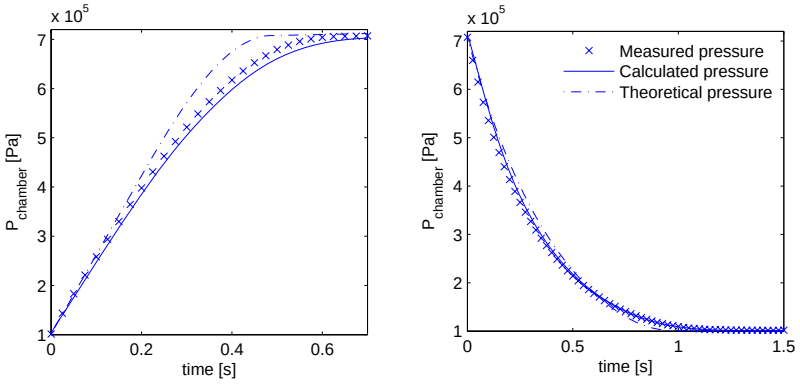

Figure 3.5. Chamber pressures, theoretical and real. Left figure is the charging process and right figure is the discharging process.

on time but on the pressure differences between the supply and chamber or the chamber and the atmosphere. Due to the fact that the supply pressure and the atmosphere pressures are constant, the flow of mass and temperature, ϵ, are functions only of the chamber pressure,

$$\epsilon_i = f(P_i) \qquad for\ i = 1, 2 \tag{3.21}$$

If the flow of mass and temperature is used instead of the mass flow, T can be eliminated,

$$\epsilon = T\dot{m} \tag{3.22}$$

resulting in a new equation for the pressure derivative,

$$\dot{P} = \alpha_m \frac{R_{air}}{V}\epsilon - \alpha\frac{P}{V}\dot{V} \tag{3.23}$$

By now, the observant reader is wondering about the α_m term discussed in 3.1.2. Are not the characteristics of the pressure change due to mass flow incorporated in the flow of mass and temperature? No, not entirely. As mentioned, the α_m term depends on the process nature of the charging/discharging process. This yields $\alpha_m = 1$ after the piston movement is completed and the remaining process only consists of filling an empty volume, as done in this section. However, this is not the entire truth. The piston movement results in turbulence and heating/cooling of the chamber air. The turbulence obstructs the inflow of air and therefore obstructs the pressure rise.

Heating of the chamber air, is a result of the piston hitting the chamber wall. The energy surplus from the moving piston has to be accounted for. Since energy can be neither created nor destroyed, the energy from the abrupt stop is transformed into heat energy warming the chamber air which results in increased pressure.

Heating/cooling is also a result from chamber reduction/expansion during piston movement. This change in temperature remains after the piston movement is complete, and effects the filling/emptying process of air, in contrast to if only a fixed volume of air is to be filled.

How the system is affected by these phenomena is hard to determine. In experiments these phenomena can not be observed, only their effect on the observed pressure, explaining -somewhat- the α_m term.

3.1.5 Friction

The friction working on the piston and the stay consists of the static and dynamic friction forces between the piston and cylinder and the stay and cylinder. Using the same notation as Richer and Hurmuzlu, [18], The total friction force is given by:

$$F_{friction} = \begin{cases} F_{sf} & \text{if } \dot{x} = 0 \\ F_{df} sign(\dot{x}) & \text{if } \dot{x} \neq 0 \end{cases} \tag{3.24}$$

The static friction is the friction acting on the piston at zero velocity. To measure this friction a piston stroke is carried out and the net force measured at the moment the piston starts to move is obtained by dividing the chamber pressures with their respective piston area. Figure 3.6 shows the force versus piston velocity and at which force the piston starts to move. The static friction is measured to 71 N.

According to Richer and Hurmuzlu, [18], dynamic friction can be modeled as an affine function, $F_{df} = F_{rf} + \beta\dot{x}$. To determine the dynamic friction, piston strokes with two different supply pressures are carried out while measuring pressure and piston position. Two different supply pressures are used to cover as large piston velocity span as possible. Acceleration and velocity of the piston is obtained by differentiating the position measurements over time. By using position measurements in the interval where the piston has started to move considerably, see Figure 3.7, the dynamic friction can be estimated.

With the piston acceleration, a, and the net applied force, the friction force is

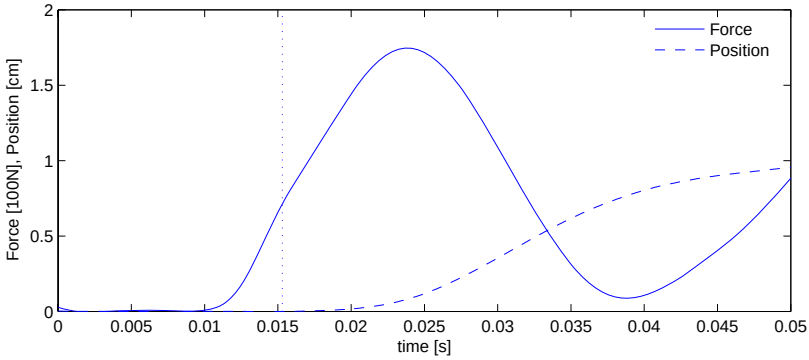

Figure 3.6. Net applied force and piston position vs. time.

obtained as,

$$F_f = F_{pressure} - a(m_s + m_p) \tag{3.25}$$

In the right part of Figure 3.7 the friction force is plotted against piston velocity.

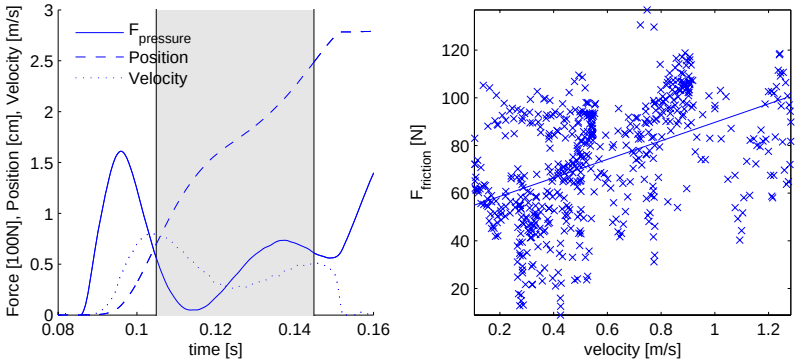

Figure 3.7. The grey interval in the right figure indicates the data used for friction measurements. In the right figure, dynamic friction vs. piston velocity is shown.

The two parts of the dynamic friction, β and F_{rf}, are identified as the slope and the offset, respectively, of the affine function that best fits the measured data in a least square sense. The obtained values are presented in Table 3.1. It is obvious that the friction model derived here is not very reliable since the measurement samples are diverse and do not really fit the first order friction model.

Friction is generally hard to determine, here the major problem is the short stroke of the piston, (1,285 cm). The short stroke length gives a short timeframe for the piston to accelerate, and the velocity span and timeframe where friction can be measured is therefore limited. Important to mention is that the piston acceleration is obtained by differentiating the position measurements twice. This

amplifies measurement noise, even if the measured data is filtered to remove high frequency components (noise). The noise amplification is clearly visible in Figure 3.7 where the measured data points are widely scattered.

Dynamic friction	
β	38.8 [Nm/s]
F_{rf}	50.9 [N]

Table 3.1. Dynamic friction coefficients.

3.2 Oil damper

Since the aim of this paper is to investigate the possibility to remove the oil damper, a model of it is only of secondary interest. It is more interesting to see how it works and how a replacing system should behave. Therefore there is no validation done for the oil damper. Further, the parameter estimation is done by hand without minimization of the mean square error. The parameters are estimated in the sense that the simulated position shall follow the measured position.

The oil damper, Figure 3.8, is similar to a hydraulic actuator and therefore theory from this field can be used to model the damper. Modeling hydraulic actuators is done by several researchers. [25, 13, 23, 2, 5], all use theory presented by Merritt, [12], for fluid flow through valves. The approach is similar here. To understand the system it is important to go through it thoroughly, this is done using Figure 3.8. When a force is applied to the piston, it starts to move and oil

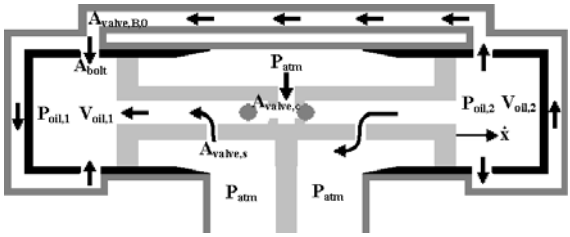

Figure 3.8. Schematic picture of the oil damper.

is forced through the two valves. Since the flow out from the second chamber is limited by the valve areas the fluid pressure will increase rapidly and produce a counteracting force. When the first valve is crossed the outflow from the chamber is limited to the smaller valve and the flow is reduced. Hence the counteracting force increases. To keep chamber one passive there is a spring type relief valve that fills chamber one with oil from an oil supply at atmospheric pressure, keeping the pressure in this chamber at the low pressure required to keep the spring valve open.

The system dynamics for the piston, neglecting friction, and with the notations from Figure 3.8 is,

$$F_{oil} = (P_{oil,2} - P_{oil,1})A_{oil} = \Delta P A_{oil} \tag{3.26}$$

For chamber two, the effective area where oil can leave the chamber consists of the two outlet holes $A_{valve,S}$ and $A_{valve,B}(x)$ where the outlet area of the B valve depends on the piston position. $A_{valve,B}(x)$ is constant until the joined area of the A_{bolt} holes is smaller than $A_{valve,B,0}$, at distance x_r.

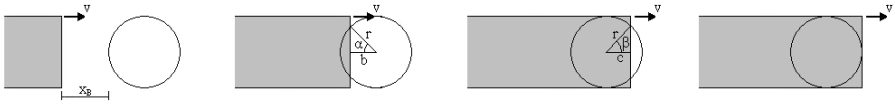

Figure 3.9. Valve area calculation.

Using notations from Figures 3.8 and 3.9, the expression for the effective outlet area $A_{valve}(x)$ becomes,

$$A_{valve}(x) = \begin{cases} A_{valve,S} + A_{valve,B,0} & \text{if } x \leq x_r \\ A_{valve,S} + 2(A_{bolt} - \alpha r^2 + rb\sin\alpha) & \text{if } x > x_r \ \cap \ x \leq x_B + r \\ A_{valve,S} + 2(r^2\beta - rc\sin\beta) & \text{if } x > x_B + r \ \cap \ x \leq x_B + 2r \\ A_{valve,S} & \text{if } x > x_B + 2r \end{cases} \tag{3.27}$$

Hence, the fluid flow from the second chamber is, [12],

$$q = C_D(x, v)A_{valve}\sqrt{\frac{2}{\rho}(\Delta P)} \tag{3.28}$$

where ρ is the density and static discharge coefficient C_d is replaced with a dynamic discharge coefficient, $C_D(x, v)$. The dynamic discharge coefficient is necessary since there are two outlet holes for the oil and since it here is used to model the leakage flow. The dynamic discharge coefficient is a function of the position and velocity of the piston.

For the first chamber the process is reversed with the addition that oil can pass through the spring relief valve when the pressure is large enough to keep it open, as discussed earlier. Since the spring in the oil damper is weak, the pressure in the first chamber is close to atmospheric pressure,

$$P_{oil,1} \approx P_{atm} \tag{3.29}$$

Without leakage flow across the chambers, the continuity equation for the chamber flow is:

$$q = \underbrace{A_{oil}\frac{\partial x}{\partial t}}_{\text{flow due to volume change}} + \underbrace{\frac{1}{\kappa}V\frac{\partial \Delta P}{\partial t}}_{\text{flow due to fluid compression}} \tag{3.30}$$

With $V_{oil,1} = V_{oil,1,0} + A_{oil}x$ and the oil bulk modulus , $\kappa = -V\frac{\partial P}{\partial V}$, (3.26), (3.30), (3.29) and the flow equations, the pressure change is:

$$\dot{P}_{oil,2} = \frac{\kappa}{V_{oil,2,0} - A_{oil}x}(A_{oil}\dot{x} - q) \tag{3.31}$$

$$\dot{P}_{oil,1} = 0 \tag{3.32}$$

As mentioned by Bobrow and Lum, [2], the fluid bulk modulus and the discharge coefficients are hard to determine. They use state feedback in a numerical least squares identification algorithm, to go around this problem.

Yun and Cho, [26], makes the assumption that the damper oil can be modeled as incompressible in the case of small chamber volumes, this simplifies the problem considerably. In the incompressible case oil density is constant. Hence, the oil flow is equal to the total volume of displaced oil,

$$q = A_{oil}\dot{x} \tag{3.33}$$

To check the validity of the incompressibility assumption the oil damper is mounted to the pneumatic force actuator and a stroke is carried out. Figure 3.10

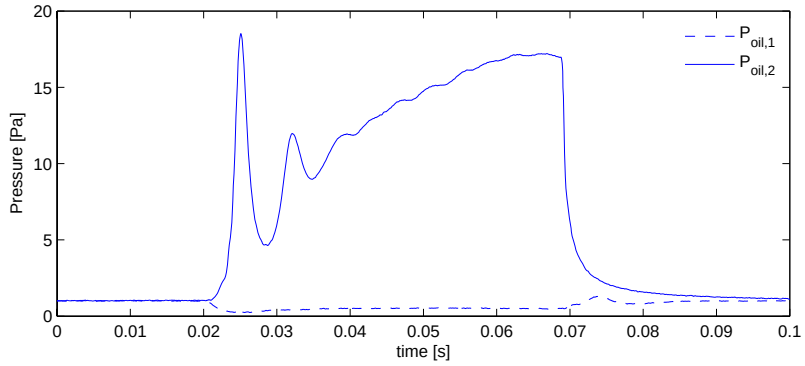

Figure 3.10. Oil damper pressure for a piston stroke.

shows the different pressures in the oil damped pneumatic force actuator setup. The compressibility is clearly visible (the pressure drop is not sudden after the piston movement is completed). However, the pressure drop is fast, the fall time from 90-20% is about 2.6 ms and the regular fall time (90-10%) is 10 ms. The small fall times indicates that the incompressibility assumption might correspond well to the theoretical case where the pressure will drop to zero as soon as the motion stops.

Figure 3.10 also confirms, as stated above, that the pressure in the first chamber is close to the pressure required to keep the spring valve open, $0.8{*}10^5$ Pa (absolute pressure) as largest. Keeping in mind that a big part of the pressure is used to keep the spring valve open and therefore not acting on the piston, and that the pressure

deviation from atmospheric pressure is much smaller than the one in chamber two, neglecting the pressure in chamber one is motivated.

With this in mind, (3.28) and (3.33) results in a new equation for the second chamber pressure,

$$P_{oil,2} = \left(\frac{A_{oil}\dot{x}}{A_{valve}C_D(x,v)} \right)^2 \frac{\rho}{2} \tag{3.34}$$

With the only unknown being, $C_D(x,v)$, it can be determined experimentally. As $C_D(x,c)$ is used to model leakage flow it is not bound to be smaller than one. The pressure drop neglected in chamber one also affects the discharge coefficient as the low pressure attracts oil from the second chamber. As mentioned, $C_D(x,v)$ is also dependent on the velocity since the amount of oil passing through the outlet holes sets the upper limit for the piston velocity. Here the dynamic discharge coefficient, $C_D(x,v)$, is chosen to be big in the beginning of the piston motion (when both outlet holes are open) and to slightly follow the piston velocity. Mainly, it is chosen so that the measured and calculated piston position are as close as possible,

$$C_D(x,v) = \max \left\{ \frac{a_{valve,B}(x)}{a_{valve,B,0}} + 0.65v \ , \ 0.65 \right\} \tag{3.35}$$

In Figure 3.11 the real system and the model are both shown. It can be concluded

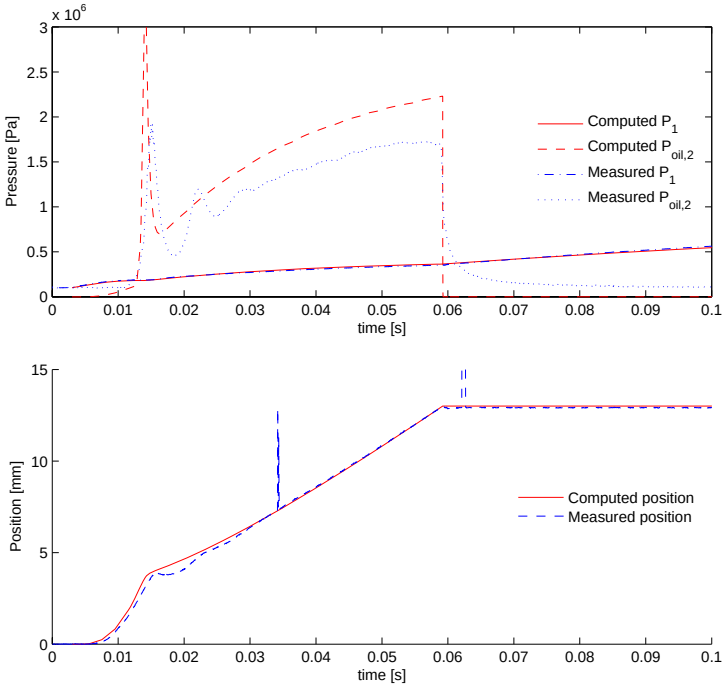

Figure 3.11. Incompressible oil damper model.

that the calculated oil pressure does not follow the true pressure, even though the measured and calculated positions follow close. The calculated pressure in the region where the oil damper acts the most is about $5 * 10^5$ Pa higher than the measured pressure. A large contribution to this digression is believed to come from friction forces introduced when the oil damper is mounted. Of interest to notice is also that the lower pressure in chamber one is neglected which of course introduces a smaller source of error.

As seen, the incompressible model does not follow the pressure fluctuations due to compressibility. Using the same outline for the discharge coefficient as in the incompressible case, but with slightly modified parameters, what can be done with the compressible model? According to [7], κ for a regular hydraulic oil is $1.724*10^9$, with this value for κ pressure fluctuations are still absent. The result is not much different as if the fluid is considered incompressible. In Figure 3.12, where κ is reduced 10 times, fluctuations similar to the ones seen in the measurements also appear in the model. The big difference in κ is believed to originate from air still trapped in the damper or air mixed with the oil, even if the first is considered more likely. It might be possible to remove this air if the damper is used continuously forcing air out of the system, this is however not verified.

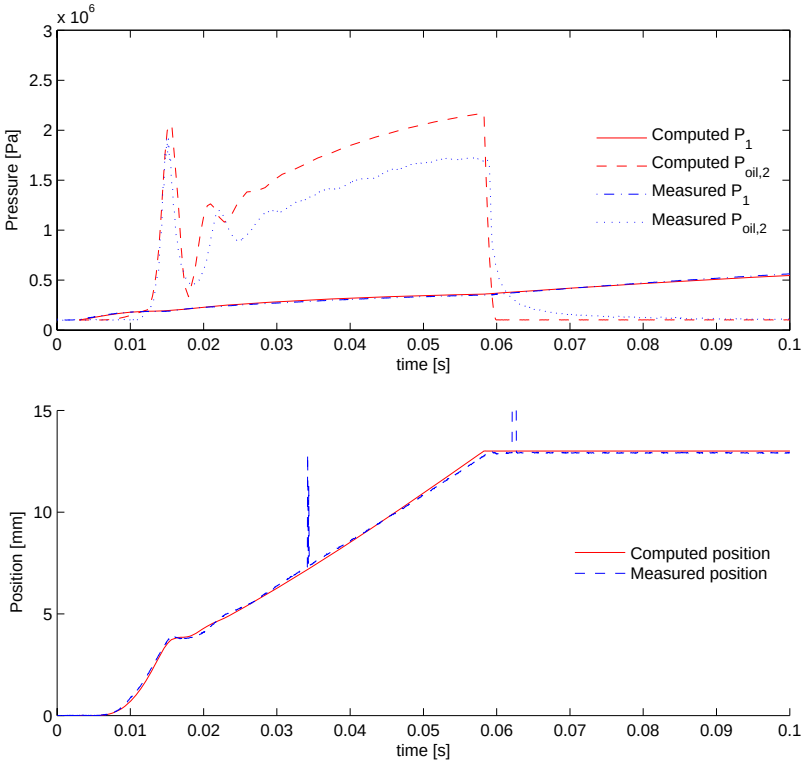

Figure 3.12. Compressible oil damper model.

3.3 System model

Using the theory presented in [11], state spaces for the two different setups, the fixed piston and the length stroke pneumatic actuator are created. As the goal is to remove the oil damper only the pneumatic part is considered from here on, this will also be referred to as the model.

3.3.1 Fixed piston pneumatic force actuator

The differential algebraic equation (DAE) for the pneumatic block is set up using (3.1), (3.23), (3.21), together with the notations from Figure 3.1.

$$\ddot{x} = \frac{1}{(m_s + m_p)} \left(P_1 A_1 - P_2 A_2 - P_{atm} A_{stay} + F_{friction}(\dot{x})\right) \quad (3.36)$$

$$\dot{P_1} = \alpha_{m,1} \frac{R_{air}}{V_1} \epsilon_1 - \alpha_1 \frac{P_1}{V_1} \dot{V_1} \quad (3.37)$$

$$\dot{P_2} = \alpha_{m,2} \frac{R_{air}}{V_1} \epsilon_2 + \alpha_2 \frac{P_2}{V_2} \dot{V_2} \quad (3.38)$$

$$\epsilon_1 = f(P_1) \quad (3.39)$$

$$\epsilon_2 = f(P_2) \quad (3.40)$$

$$V_1 = A_1 x + V_{1,0} \quad (3.41)$$

$$V_2 = V_{2,0} - A_2 x \quad (3.42)$$

$$\dot{V_1} = A_1 \dot{x} \quad (3.43)$$

$$\dot{V_2} = -A_2 \dot{x} \quad (3.44)$$

$$F_{friction} = \begin{cases} F_{sf} & \text{if } \dot{x} = 0 \\ F_{df} sign(\dot{x}) & \text{if } \dot{x} \neq 0 \end{cases} \quad (3.45)$$

Transferring the system to first order by introducing $x_1(t) = x(t)$, $x_2(t) = \dot{x}(t)$, $x_3(t) = P_1(t)$ and $x_4(t) = P_2(t)$ and with the control signals $u_1(t)$ and $u_2(t)$ for valve one and two respectively (1 = open, 0 = closed). The final DAE state space can be simplified to:

$$\dot{x}_1 = x_2 \quad (3.46)$$

$$\dot{x}_2 = \frac{1}{(m_s + m_p)} \left(P_1 A_1 - P_2 A_2 - P_{atm} A_{stay} + F_{friction}(x_2)\right) \quad (3.47)$$

$$\dot{x}_3 = \alpha_{m,1} \frac{R_{air}}{(A_1 x_1 + V_{1,0})} \epsilon_1 - \alpha_1 \frac{x_3}{A_1 x_1 + V_{1,0}} A_1 x_2 \quad (3.48)$$

$$\dot{x}_4 = \alpha_{m,2} \frac{R_{air}}{(V_{2,0} - A_2 x_1)} \epsilon_2 + \alpha_2 \frac{x_4}{V_{2,0} - A_2 x_1} A_2 x_2 \quad (3.49)$$

$$\epsilon_1 = u_1 f_1(x_3) + (u_1 - 1) f_2(x_3) \quad (3.50)$$

$$\epsilon_2 = u_2 f_2(x_4) + (u_2 - 1) f_1(x_4) \quad (3.51)$$

$$F_{friction} = \begin{cases} F_{sf} & \text{if } x_2 = 0 \\ F_{df} sign(\dot{x}) & \text{if } x_2 \neq 0 \end{cases} \quad (3.52)$$

Left are only the unknowns $\alpha_{m,i}$ and α_i for $i = 1, 2$ to be determined. To determine these, a stroke is simulated with the fixed piston pneumatic force actuator model. Pressures in chamber one and two are recorded as well as the stay (piston) position. It is then compared to real values of the same stroke in the lab setup. The constants are chosen so that the system model is as close to the real system as possible (regarding chamber pressures), in a mean square sense (MSE), with the results presented in Figure 3.13. The coefficients that best match the theoretical model

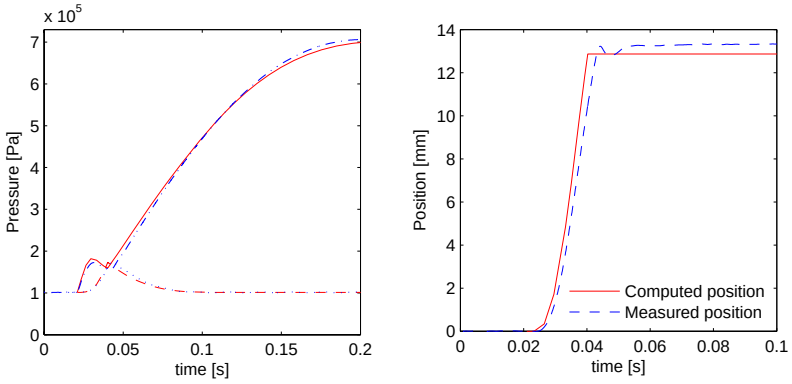

Figure 3.13. Simulated and measured piston stroke.

to the real process are shown in Table 3.2. One can conclude that the charging process follows closer to the isothermal process. The discharging process however is a bit trickier. The first part (while the piston is moving), which mainly consists of the compression of air follows close to the isothermal process. In the second part, mainly consisting of emptying the cylinder, $\alpha_{m,2}$ is large. The authors believe that the explanations given in 3.1.2 and 3.1.4 for the α_m term is the main reason for this. These conclusions should be put in context with the process time, which is about 200 ms. Important to notice however, is that the piston movement is over in 15 ms. The rest is merely filling of an empty volume.

$\alpha_{m,1}$	0.94
α_1	0.87
$\alpha_{m,2}$	1.5
α_2	1.05

Table 3.2. $\alpha_{m,i}$ and α_i for $i = 1, 2$.

3.3.2 The length stroke pneumatic force actuator

The length stroke pneumatic force actuator differs a bit from the fixed piston setup discussed earlier. The length stroke pneumatic force actuator consists of two

pistons, that can move freely (a short distance) on the stay, and three chambers. A schematic picture is shown in Figure 3.14. There are four different shifting possibilities: neutral to backward, backward to neutral, neutral to forward and forward to neutral. The dynamics for these shifts are very similar, therefore only shifting from neutral to backward is be presented here.

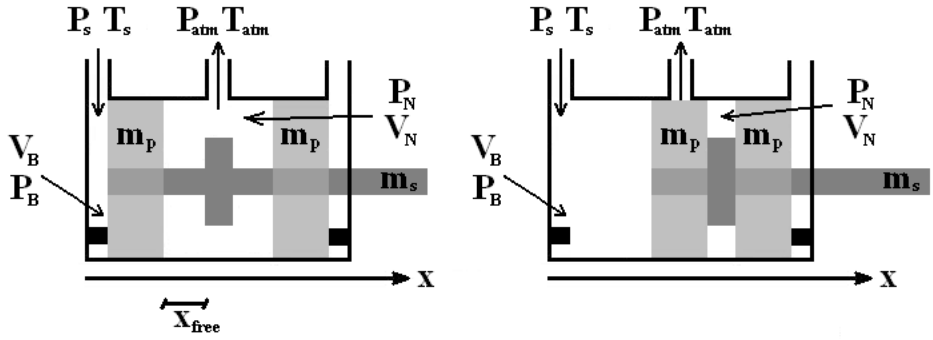

Figure 3.14. Schematic picture of a gear shift (neutral to back), in the length stroke pneumatic force actuator.

However, as shown in Figure 3.14 one of the pistons is fixed during the gear shifting process. This is always the case when a gear is shifted, regardless of current position and the position it is shifted to. The length stroke is therefore equal to the system presented earlier with the exception that the piston moves freely on the stay until it attaches after moving a relative (to the stay) distance, x_{free}. It is important to note that the piston moving freely on the stay is not observable. With all of this in account, together with the friction forces on the stay, piston and the total friction force, the DAE state space for the length stroke pneumatic force actuator becomes,

if $x_{free} > 0$

$$\dot{x}_s = v_s \tag{3.53}$$
$$\dot{x}_p = v_p \tag{3.54}$$
$$\dot{v}_p = \frac{1}{m_p}\left(P_B A_p - P_N A_p + F_{f,p}(v_p)\right) \tag{3.55}$$
$$\dot{v}_s = \frac{1}{(m_s + m_p)}\left(P_B A_s - P_{atm} A_s + F_{f,s}(v_s)\right) \tag{3.56}$$
$$\dot{P_B} = \alpha_{m,B}\frac{R_{air}}{A_s x_s + A_p x_p + V_{B,0}}\epsilon_B - \alpha_B \frac{P_B(A_s v_s + A_p v_p)}{A_s x_s + A_p x_p + V_{B,0}} \tag{3.57}$$
$$\dot{P_N} = \alpha_{m,N}\frac{R_{air}}{(V_{N,0} - A_p x_p)}\epsilon_N + \alpha_N \frac{P_2}{V_{2,0} - A_p x_p} A_p v_p \tag{3.58}$$
$$\epsilon_B = u_B f_{B,in}(P_B) + (u_B - 1) f_{B,out}(P_B) \tag{3.59}$$
$$\epsilon_N = u_N f_{N,in}(P_N) + (u_N - 1) f_{N,out}(P_N) \tag{3.60}$$
$$F_{friction} = \begin{cases} F_{sf} & \text{if } v = 0 \\ F_{df} sign(\dot{x}) & \text{if } v \neq 0 \end{cases} \tag{3.61}$$

if $x_{free} = 0$

$$\dot{x} = v \tag{3.62}$$
$$\dot{v} = \frac{1}{(m_s + m_p)}\left(P_B(A_p + A_s) - P_N A_p - P_{atm} A_s + F_f(v_s)\right) \tag{3.63}$$
$$\dot{P_B} = \alpha_{m,B}\frac{R_{air}}{A_s x_s + A_p x_p + V_{B,0}}\epsilon_B - \alpha_B \frac{P_B(A_s v_s + A_p v_p)}{A_s x_s + A_p x_p + V_{B,0}} \tag{3.64}$$
$$\dot{P_N} = \alpha_{m,N}\frac{R_{air}}{(V_{N,0} - A_p x_p)}\epsilon_N + \alpha_N \frac{P_2}{V_{2,0} - A_p x_p} A_p v_p \tag{3.65}$$
$$\epsilon_B = u_B f_{B,in}(P_B) + (u_B - 1) f_{B,out}(P_B) \tag{3.66}$$
$$\epsilon_N = u_N f_{N,in}(P_N) + (u_N - 1) f_{N,out}(P_N) \tag{3.67}$$
$$F_{friction} = \begin{cases} F_{sf} & \text{if } v = 0 \\ F_{df} sign(\dot{x}) & \text{if } v \neq 0 \end{cases} \tag{3.68}$$

3.4 Model verification

If the model is to be used further for parameter analysis or control implementation it is important that the model is accurate or at least has the same properties as the real system. The verification is also a good way to find out how robust the model is. The fixed piston model is verified with two different tests, the first test is to attach the oil damper and test how well the calculated pressure in the pneumatic actuator follows the measured pressure. In the second test, a setup where a spring mounted to the stay and added to the model is compared.

The length stroke pneumatic actuator is validated doing a simulation of a stroke from neutral to backward and comparing it to the same stroke in the lab setup.

3.4.1 Method

To test the accuracy of the model, the mean relative error together with the maximum relative error is used,

$$\text{mean relative error} = \frac{1}{N}\sum_{i=1}^{N}\frac{|y(t_i)-\hat{y}(t_i)|}{|\max y(t)|} \tag{3.69}$$

$$\text{maximum relative error} = \max_{a\leq i\leq N}\frac{|y(t_i)-\hat{y}(t_i)|}{|\max y(t)|} \tag{3.70}$$

$y(t_i)$ is a measured data series, $\hat{y}(t_i)$ is the values obtained from simulation and N is the number of samples. These methods of accuracy control are of course combined with a visual study where measured and computed data are compared.

3.4.2 Position trajectory verification (fixed piston)

In this test, the oil damper is mounted and a piston stroke is carried out while pressure and position are measured. The position measurement is used as input to the model where the pneumatic actuator pressures are calculated. To be able to compare with the real measurement, the simulated model is set to act as if a piston stroke is introduced. This means that the valve is open. The result is presented in Figure 3.15 and Table 3.3.

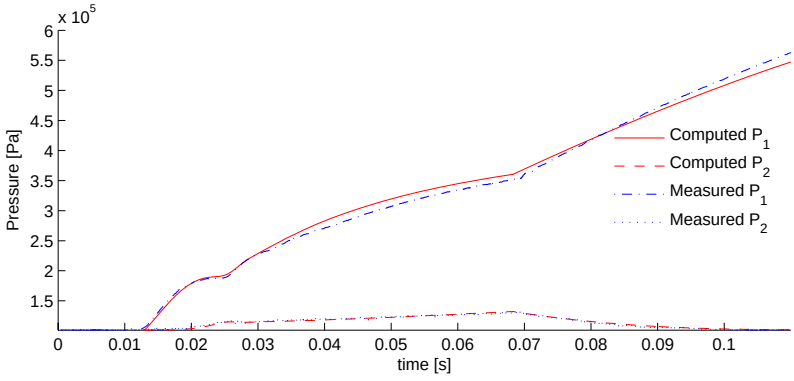

Figure 3.15. Verification using the oil damper.

The pressure build up in the simulated chambers corresponds well to the real case. This shows that the equations governing chamber pressures are accurate and can be used for parameter analysis and for control purposes.

3.4.3 Verification with spring force (fixed piston)

The second verification approach covers the entire pneumatic model. A spring force is attached to the stay, in accordance with Figure 3.16 and the volume in

Mean relative error	
Pressure in chamber 1	1.7 %
Pressure in chamber 2	3.8 %
Maximum relative error	
Pressure in chamber 1	3.5 %
Pressure in chamber 2	9.3 %

Table 3.3. Mean and maximum relative errors for the position trajectory verification.

chamber one is increased by 43% while the volume in chamber two is reduced by 16% (from original values). In Figure 3.17 and Table 3.4 the measurements from

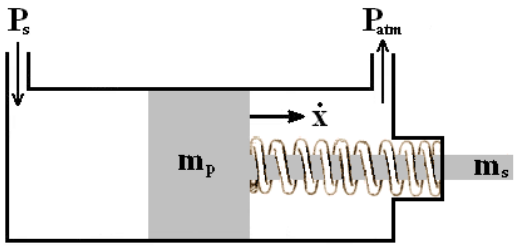

Figure 3.16. Spring force verification setup.

a piston stroke is compared to data from the model with the same spring setup.

Mean relative error	
Position	5.1 %
Pressure in chamber 1	4.3 %
Pressure in chamber 2	5.4 %
Maximum relative error	
Position	11.1 %
Pressure in chamber 1	5.9 %
Pressure in chamber 2	10.3 %

Table 3.4. Mean and maximum relative errors for the spring force verification.

The verification shows that the model is accurate even with a spring force added and with the volumes changed. The pressure build ups are equivalent, although the simulated piston movement acts in the same way as the measured movement, some delay of about 2 ms is recognized. With these results it is fair to say that the model created is robust to volume changes and externally added forces.

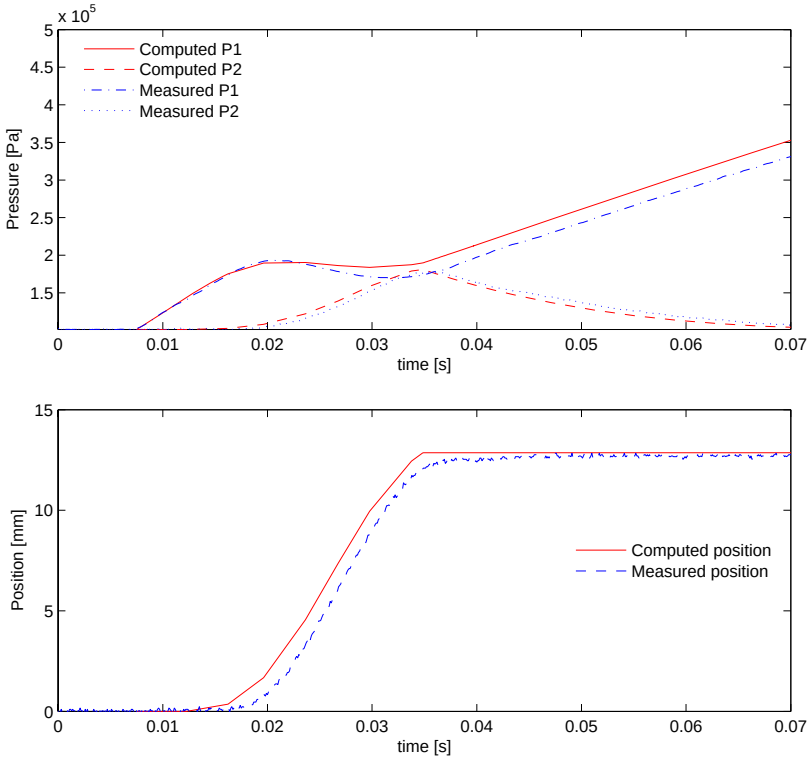

Figure 3.17. Model vs. real measurements with the spring force added.

3.4.4 Error sources (fixed piston)

The friction force is hard to determine and is probably the largest source of error Both the static and dynamic friction force vary between the shifts and it is hard to see the linear dependence between the velocity and the friction in Figure 3.7. Another source of error relating to the spring validations is that no extra friction force has been added to the model. The friction from the spring is small and can presumably be neglected but might be a small source of error.

In given trajectory validation, friction is accounted for since the position is used as an input to the simulation. By comparing the other validations with this one, a comprehension of how the friction force affects the system, and how accurate the friction model is, is obtained. It can be concluded that the friction model is far from perfect and that the friction forces are probably underestimated.

The chamber pressure dynamics is probably the second largest source of error. As presented in 3.1.2 no formulas exist for pressure and temperature calculations at the same time or any certain way to determine the exact process nature. Since both the verification processes are slower than the fixed piston system, it is likely that the α terms corresponding to the process (adiabatic / isothermal) changes

with the lower system velocity.

The spring, used in 3.4.3, itself introduces another error. The spring force is modeled as proportional to the piston displacement (a linear spring model). This is of course not correct but a good estimation, since accurate spring data is available.

Cheap and poor equipment is often a big source of error. Here a high sampling rate and high standard equipments are used to eliminate these kinds of error sources.

3.4.5 Length stroke pneumatic force actuator verification

To test the Length stroke pneumatic force actuator a gear shift from neutral to backward is carried out. The result is shown in Figure 3.18 and Table 3.5.

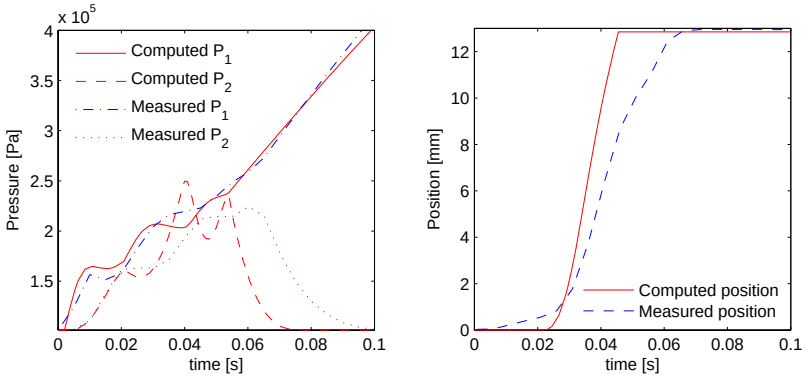

Figure 3.18. Gear shift with the length stroke pneumatic force actuator, neutral to backward.

Mean relative error	
Position	10.1 %
Pressure in charging chamber	2.2 %
Pressure in discharging chamber	17.8 %
Maximum relative error	
Position	34.0 %
Pressure in charging chamber	5.4 %
Pressure in discharging chamber	76.7 %

Table 3.5. Mean and maximum relative errors for the length stroke pneumatic force actuator.

The result is not convincing: the simulated piston movement is to fast compared to the real measurements. The effect of this is clearly visible also on the chamber pressures. In Figure 3.18, the pressure in the passive chamber rush since the piston movement is very fast. To see if friction is a big error factor, another simulation is performed with increased friction (dynamic friction increased three times), see Figure 3.19, and Table 3.6.

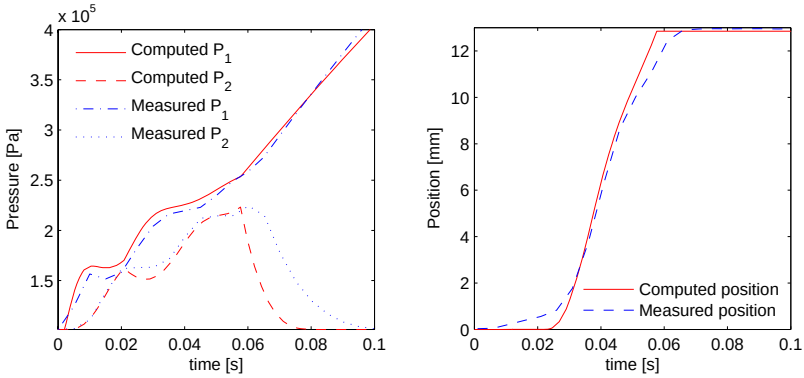

Figure 3.19. Gear shift with the Opticruise pneumatic force actuator, neutral to backward with adjusted frictions.

Mean relative error	
Position	2.8 %
Pressure in charging chamber	2.1 %
Pressure in discharging chamber	10.6 %
Maximum relative error	
Position	9.9 %
Pressure in chamber 1	5.2 %
Pressure in chamber 2	62.4 %

Table 3.6. Mean and maximum relative errors for the length stroke pneumatic actuator with increased friciton.

It clearly shows that the friction lies behind a large part of the differences between measured and simulated data as discussed previously in 3.4.4. However, this does not exclude the possibility of other error sources.

Chapter 4

Gear shifting in truck

In previous chapters, work is done modeling the length stroke. As mentioned, modeling is done on a length stroke detached from the corresponding gearbox. The model gives good knowledge of the mechanics behind the length stroke but not so much regarding gear shifts while operating, mounted to a gearbox in a truck.

During such conditions, the force, pressure and time required to shift gears differs from the ideal conditions used when modeling. To be able to draw conclusions on how to improve (i.e. minimize gear shift time, improve comfort and reduce cost) the length stroke, it is necessary to study it during normal working conditions. Since the goal is to remove the oil damper it is important to see how the system works without it; all gear shifts in truck are done without the oil damper.

However, mounting the length stroke to a truck raise new problems. The more accurate external position sensor can not be mounted. Hence all conclusions must be drawn studying the pressure in the pneumatic actuator combined with the less accurate internal position sensor.

4.1 Gear shifting

As understood by now, Opticruise is more than a pneumatic system which replaces the physical work of the driver when shifting gear. When shifting gear the torque transferred in the driveline is first controlled to zero, in reality only close to zero since the engine torque can not be determined accurately. This makes it possible to pull the current gear out smoothly and place the gearbox in neutral position. Since the torque does not always reach zero, high forces/pressures are sometimes required to disengage the gear. The required forces are not known in advance which makes the model inaccurate and complicates when control strategies are constructed for the length stroke.

When the gear is in neutral, engine speed is synchronized to fit the higher gear. As soon as correct speed is reached next gear is engaged and the engine torque can be controlled back to the torque requested by the driver. The synchronization

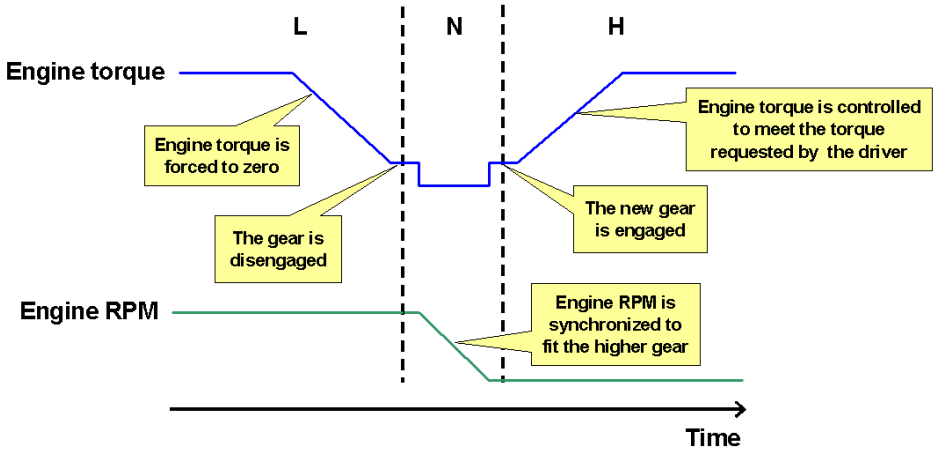

Figure 4.1. Gear shift from a lower to a higher gear.

is not perfect, therefore the angular velocity of the engine and driveline are not equal. An overwiev of the gear shifting process is illustrated in Figure 4.1.

4.1.1 Synchronization

Every driver of manual gear shifted car knows that there is a certain amount of force required to engage and disengage the gear when shifting. Sometimes the gear is engaged smoothly and sometimes a larger force is required. Commonly, there is a force barrier to overcome the first bit, thereafter the rest of the movement follows smoothly. This is also the case with the Opticruise gearbox. Here this force arise from the synchronization process in the gearbox.

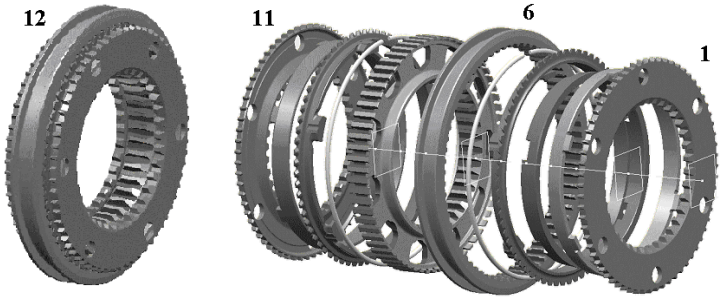

Figure 4.2. To the left, a double and single synchronizer. To the right, its corresponding exploded view.

In a Opticruise controlled gearbox there are triple, double and single synchronizers. Here, only the single and double synchronizers are discussed. A double and

single synchronizer is shown in the left part (12.) of Figure 4.2. To understand the synchronization process and the construction, it is favorable to follow the exploded view in the right part of Figure 4.2. The names of the different parts, using the notation from Figure 4.2 (1-11, from right to left) are:

1. coupeling disc
2. middlecone
3. innercone
4. latchcone
5. treadring
6. coupeling sleeve
7. driver
8. treadring
9. latchcone
10. middlecone
11. coupling disc

The double synchronizer consists of parts 1-5 while 8-11 represents the single synchronizer. Parts 6 and 7 are common for both synchronizers. When shifting gear, the length stroke puts force on the coupeling sleeve and moves it towards the coupeling disc. The relative angular velocity difference between the coupeling sleeve and coupeling disc is reduced in the middlecone and the latchcone, or if it is a double synchronizer, between the middlecone, the innercone and the latchcone. The difference in angular velocity originate from the different angular velocities between engine and driveline. When the angular velocities between the coupeling sleeve and the coupeling disc are equal, the coupeling sleeve passes the latchcone and attaches to the coupeling disc, completing the gear shift.

The force required to perform the synchronization process is different in every gear shift and can not be determined in beforehand because of the inaccurate synchronization of angular velocities between engine and driveline.

4.2 Control

Commonly, pneumatic actuation is used to produce motion between two hard stops. However, in later years, pneumatic actuation has been popular in robotic applications due to their power output to cost ratio and the availability of compressed air in combination with improved methods for position control of such devices.

In the length stroke, fast pneumatic actuation between two hard stops is required, but it is also important not to hit the hard stops with high velocity, a problem which until now has been solved with the oil damper. Three ways of solving this problem are looked at. First the idea of developing a position feedback controller is discussed. Second, a strictly model predictive controller is looked at and third, a mechanical approach where the point is to make the pneumatic actuator mimic the oil damper.

4.2.1 Position feedback control

Work on position control of pneumatic actuators is done by several researchers. Bobrow and Mcdonell, [3], and Rao and Bone, [17], use feedback of both chamber

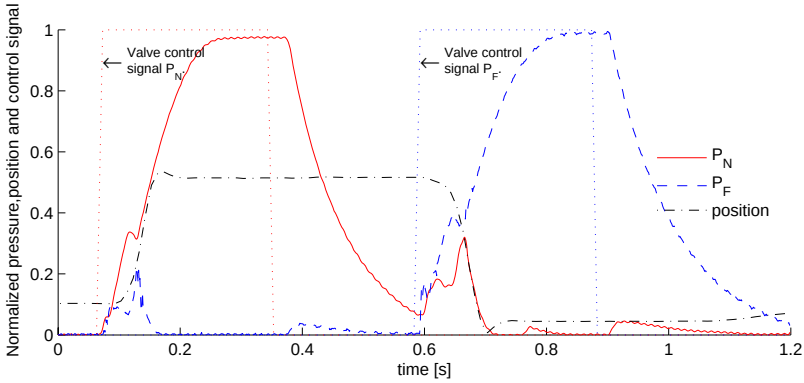

Figure 4.3. Gear shift from neutral to forward.

pressures and piston position, which of course is favorable but not possible here since pressure gauges are not available for the length stroke (apart from the test setup).

Paul et al., [15], develops a reduced order sliding mode controller using only the piston position as feedback information, they also use on/off solenoid valves. However, the pneumatic actuator used by Paul et al., [15], is big and slow compared to the length stroke. Furthermore, the length stroke differs from other pneumatic actuators in the sense that the synchronization resistance from the gearbox is unknown, making the required pressure unknown and different in time.

Figure 4.3 shows a typical gear shift from neutral to forward. The effective time required to pull/push the gear out/in (the time interval where the stay and the piston move together) can be obtained. This time interval hint if it is at all possible to apply some sort of feedback control before the process is over. Studies of numerous gear shifts show that this time interval typically is between 40-100 ms when switching to neutral and between 70-120 ms when switching to forward or backward. That the shifting interval is so different from time to time follows from the different conditions in the gearbox at every different gear change, discussed earlier.

The aim of the pneumatic feedback control is to replace the oil damper with a feedback control law. As discussed in 3.2 the oil damper is designed to reduce wear when shifting gear from neutral to backward/forward. Hence, it is interesting to compute feedback control only when gear is shifted in this way. From above it follows that the limiting time is 70 ms. In this time interval a feedback control must be fast enough to mimic the behavior of the oil damper by controlling the air flow to the chambers on both sides of the piston.

The problem originating from the unknown force from the synchronization is seen in Figure 4.4, where the piston-stay does not move smoothly, but stops while passing the synchronizers. In this case, if the first samples from the position sensor is used to calculate speed and velocity and the control output is built on these data, the result will not be favorable for the gear shifting process. It is possible to come

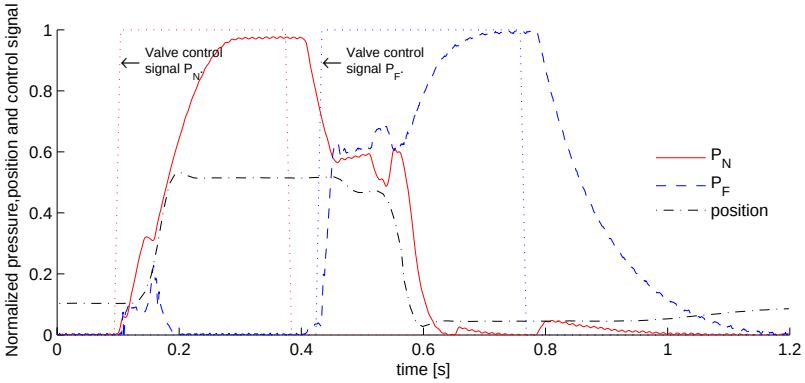

Figure 4.4. Piston movement stops during gear engagement.

around this problem, in the last part of the gear shift, when the coupeling sleeve has just started to pass over the coupeling disc, the system dynamics are similar to the dynamics derived in Chapter 3. If the problem is reformulated so that control strategies are applied at this point, the uncertain factor in the model introduced with the gearbox is removed.

Remembering that it is important to produce fast gear shifts, optimal control comes to mind. The problem is formulated as:

$$\min \int_0^{t_f} dt, \quad \text{subj. to} \quad \begin{cases} \dot{\boldsymbol{x}}(t) = f\left(\boldsymbol{x}(t), \boldsymbol{u}(t)\right) \\ \boldsymbol{x}(0) = \boldsymbol{x}_i, \ \boldsymbol{x}(t_f) = \boldsymbol{x}_f \\ \boldsymbol{u}(t) \in \{0, 1\}, \ t_f > 0 \end{cases} \tag{4.1}$$

Here, the starting position and velocity can be given as feedback information while the chamber pressures must be estimated. Choosing fixed final states is no problem for position and velocity, it is more tricky for the chamber pressures. Since the aim is to minimize the gear shifting time it is important to choose the final states for the pressures so that they do not affect the overall performance. If the final pressure in the charging chamber is chosen as the reservoir pressure, and for the discharging chamber atmosphere pressure, a autonomous system (fixed initial and final states) is obtained. This optimization problem is a special case of Pontryagin's minimum principle (PMP). How to solve such a optimization problem is discussed in [8]. However, before this is done it is important to look at some fundamental limitation to see if a feedback control law can be utilized.

The Opticruise control unit, OPC4, samples at 100 Hz frequency, i.e. every 10 ms. This gives a total of 7 samples to work with during the process. Reasonable feedback information is the piston-stay position and velocity. To calculate the velocity at least two samples are necessary. This in consideration with the inaccuracy of the position sensor is problematic when trying to feedback control a fast process like this.

Further problems arise when pneumatic feedback control is considered, the on/off solenoid valves discussed in 3.1.3 are slow and have an opening delay of about 8 ms and a closing delay of about 35 ms. In the same way as above this is also problematic when developing a fast pneumatic feedback control. The single largest drawback comes with the position sensor, which is discussed in 2.2.4. It comes with a 30 ms delay which is of course devastating seen from a control perspective.

To sum up, the time space for control of the last part of the piston movement, can be around 40 ms in a decent scenario. When the measured position reaches the OPC4 30 ms has past. Sampling with the OPC4 unit at 100 Hz and calculating the velocity from only 2 samples costs another 10 ms. Opening the valve takes 8 ms. At that time the piston is already at the end position. Note that the problems occurring with the long closing time of the valve are not even discussed.

Considering all the drawbacks presented, the conclusion can be none other than that the OPC4 (with the current software setup), the position sensor and the solenoid valves are not adequate to support a position feedback control solution.

4.2.2 Model predictive controller

A model predictive control law requires good knowledge of how the system behaves, i.e. a good model of the system. In Chapter 3 a model for the length stroke is derived. Using this model it might be possible to construct some sort of model predictive control scheme, to mimic the oil damper. However, still some of the problems mentioned in 4.2.1 remains.

The idea to use a model predictive control scheme collapses in the same moment as the length stroke is mounted in a gearbox in a truck. In the lab environment where the model of the length stroke is constructed, no external force is applied to the length stroke. When the length stroke is mounted on a gearbox in a truck, there is suddenly the external force from the synchronizers. The external force itself is not a problem, the problem is that it is not known. It is different in every gear shift, and depend on factors like differences in torque and RPM between the gearbox and the engine as discussed earlier.

Data acquired from gear shifting in truck shows that this external force ranges from almost nothing up to 2.2 kN. A system like this, where the system properties are highly fluctuating, is not a good candidate for any sort of model predictive control. However, this does not imply that the model derived in previous sections is worthless. In Chapter 5 the model is used to help understand how, if possible, desirable system properties can be obtained.

4.2.3 Mechanical control

In previous sections, it is concluded that the system is either to fast to candidate for feedback control, using existing equipment or to variable for a model predictive control approach. The conclusion is that something different is needed, something fast and independent of variable synchronization forces. Today, the solution is the oil damper which slows the process considerably during the last stage of the gear

shift. This is indeed a working mechanical controller; but, since it is expensive, it is desirable to work out if it is possible to find a cheaper construction.

Ideas for a cheaper construction where a pneumatic approach is considered is discussed in Chapter 5 and Chapter 6.

Chapter 5

Effects of hardware parameters

With the model derived in Chapter 3 it is easier to understand how different hardware setups change the system properties. Some parameters are obviously interesting to look at, like the piston radius which is decisive when pressure is transformed into force and the initial and final volumes of air in the chambers. Furthermore, piston mass and the air inlet holes are regarded. Throughout this chapter, the fixed piston pneumatic actuator from Section 3.3.1 is used to analyze how these hardware parameters affect the system.

5.1 Piston radius

The pressure to force transformation is perhaps the first thing coming to mind when regarding the piston radius. This relationship is given by,

$$F = PA = P\pi r_{piston}^2 \tag{5.1}$$

where the force is proportional to the square of the piston radius. Therefore, increase in radius has a high impact when pressure is transformed into force. Likewise, if the radius is decreased, a lot more pressure is required to obtain the same force.

Another effect of the piston radius is the chamber volume which vary with the radius according to,

$$V_{chamber} = Ax = \pi r_{piston}^2 x \tag{5.2}$$

with the same conclusion as above, the chamber volume is proportional to the square of the radius. The quick observation is the trade-off between force and chamber volume. This is indeed true, but there are more aspects to view. Of course larger chamber volumes require more time for filling which slows the pressure rise and convey larger pressure drops when the piston is moving and the volume is

expanding. But, larger chamber volumes affect both sides of the piston. A larger piston radius bring a larger initial volume in the passive chamber; when this volume is reduced, due to piston movement, the pressure rise in this chamber becomes much higher since a larger volume of air is compressed. Depending on the chosen radius, effects on the overall performance are high. Figure 5.1 shows how different piston radii affect the fixed piston pneumatic actuator derived in 3.1.

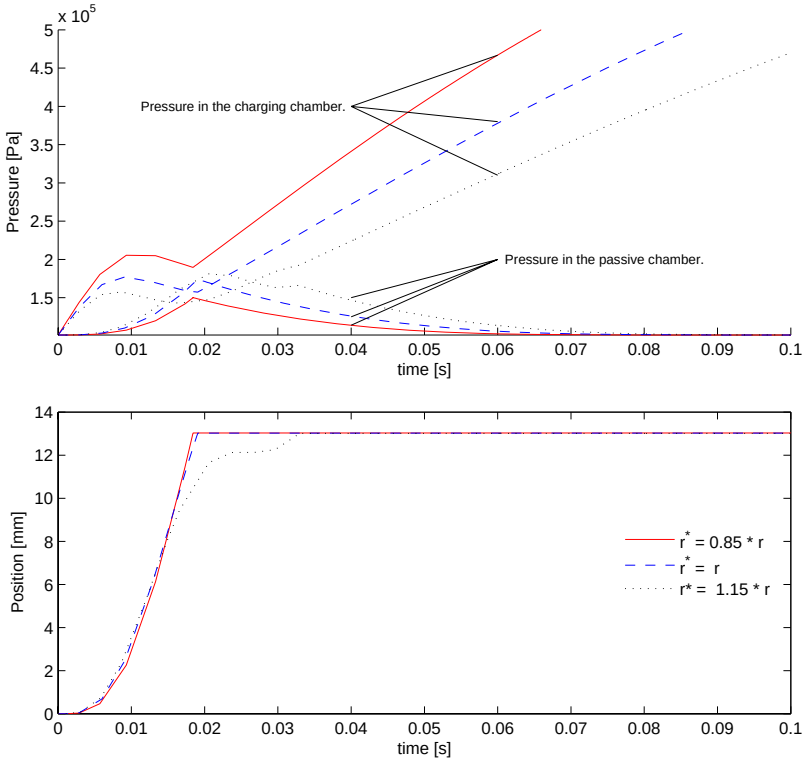

Figure 5.1. Influence of piston radius in the fixed piston system.

Interesting to note from Figure 5.1 is not that the pressure required is proportional to the square of the piston radius, this is already discussed. Interesting to observe is how the increased start volume in the passive chamber together with the higher pressure rise in this chamber due to the faster volume reduction (larger radius gives a higher piston area which makes the influence of the piston position much larger) affects the system.

The reason for the high pressure build up in the passive chamber is mainly the unchanged outlet holes, in comparison with the increased piston area. In this case, the result is much more interesting than the explanation. As observed, the piston speed is reduced to zero close to the end position only by the pressure build up in the second chamber and friction forces. This resembles the work done by the oil damper and is therefore of interest. However, as hinted in Figure 5.1 and

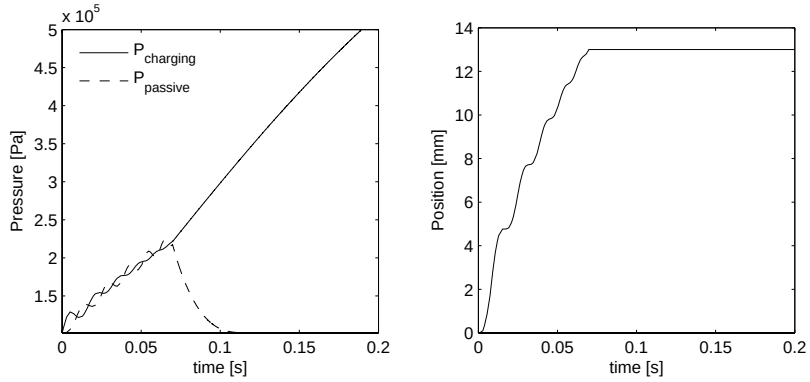

Figure 5.2. Fixed piston system properties in the case of a large radius.

shown in Figure 5.2 large piston areas causes oscillations in the piston position and therefore produce slower systems. So there is a trade-off between the positive breaking effect caused by the large area and the oscillations it produces.

5.2 Initial and final volumes

This section goes hand in hand with the previous section where larger piston areas are discussed. It is stated that systems using larger piston areas requires less pressure and result in larger pressure build up in the passive chamber, but also tend to get a oscillating behavior. Rational choices of initial and final volumes, might make the results from the previous section easier to use.

5.2.1 Initial volume

Initial volume is the term for the initial volume of air in the chamber undergoing a charging process. A more detailed description is obtained by looking at Figure 5.3.

The initial air volumes contributes to the system in two ways. Using (3.23) from 3.1.2 it can be concluded that a small initial volume gives a faster pressure build up but also a faster pressure drop when the chamber is expanding due to the more rapid volume increase. A larger initial volume acts in the opposite way, the larger volume will take more time to fill, therefore a slower pressure build up. But when expanding, the pressure drop will not be as big, since the chamber volume is not expanding rapidly in size. Using the model from the fixed piston pneumatic force actuator these fenomena are shown in Figure 5.4.

Using the double pistoned length stroke, influence of the initial volume is limited. This is due to the piston, which moves freely in the beginning of the process, creating a relatively large volume before the pressure build up affecting the gearbox starts. A smaller initial volume might speed up this freewalk, but it would

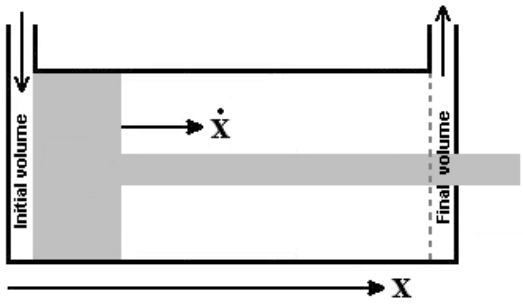

Figure 5.3. Initial and final volumes.

merely save milliseconds in the process.

The initial volume is more interesting to regard in a single (fixed) piston system, where the advantage of a fast pressure build up can be utilized. In a single (fixed) piston system, force applied to the piston is directly transferred to the stay and exerted on the gearbox.

5.2.2 Final volume

This area is somewhat introduced in 5.1, the increased radius size increases the ratio between initial and final air volume and therefore acts in the same way as if the final volume is reduced.

Increasing the final volume has the effect that the pressure build up in the passive chamber due to piston movement is smaller and therefore less significant due to the reduced effect on the system; i.e. a infinite final volume will make it possible to neglect the influence of the second chamber, since there will be no pressure change.

As hinted in 5.1, reducing the final volume is more interesting. If the final volume is small (close to zero) the pressure build up in the passive chamber will be high in the end of the piston movement. The result is that the passive chamber, in case of well designed outlet holes, can act as the oil damper and reduce the piston velocity when it is close to the end position.

In Figure 5.5 the fixed piston system is simulated with the normal final volume, the final volume reduced ten times and increased ten times. It clearly show the effect of a smaller and larger final volume.

5.2.3 Small volumes

Concluding previous sections, it seems beneficial to use small final and start volumes. The fixed piston pneumatic actuator with small final and start volumes (reduced ten times in comparison to their original value) are simulated with the result shown in Figure 5.6.

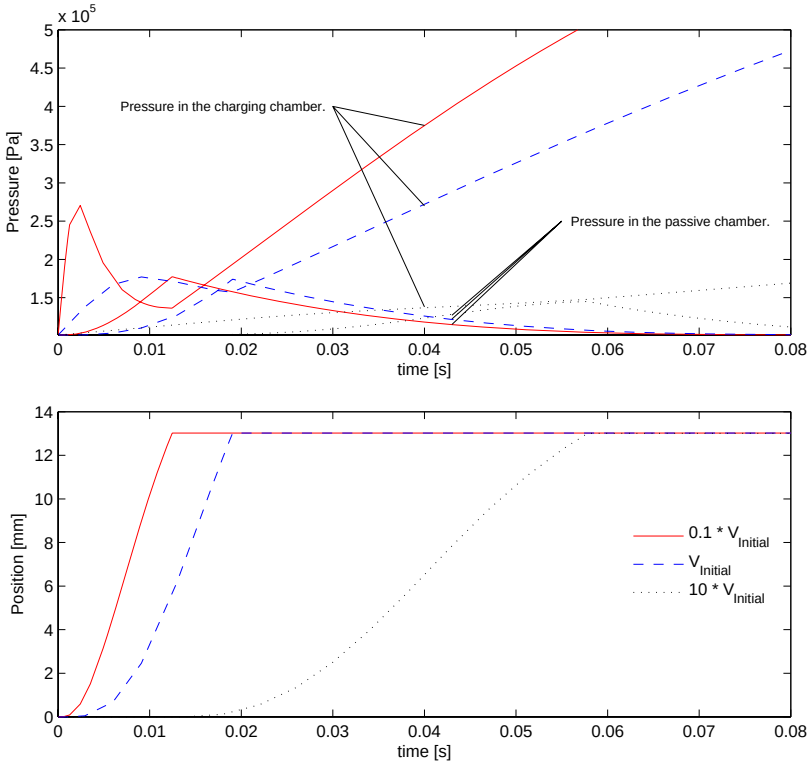

Figure 5.4. Effects of small and large initial volumes.

Figure 5.6 show that it might be possible to replace the oil damper with reduced final volumes. The small final volume will be further adressed in 6.2 where future solutions are discussed.

5.3 Piston mass

With the radius and volume part covered it is time to figure out how the piston mass affects the system behavior. To look at how the piston mass affects the length stroke on a gearbox, the fixed piston pneumatic force actuator used earlier is not applicable. This is due to the small mass of the piston in comparison to the total mass of the system when the length stroke is mounted on a gearbox. However, to show that a lighter piston does not affect the system considerably a simulation with the fixed piston system is carried out. From Figure 5.7 it is clear that a lighter piston will not affect the length stroke in a negative sense.

The piston mass is interesting in the sense that a lighter piston saves total weight, which is appreciated.

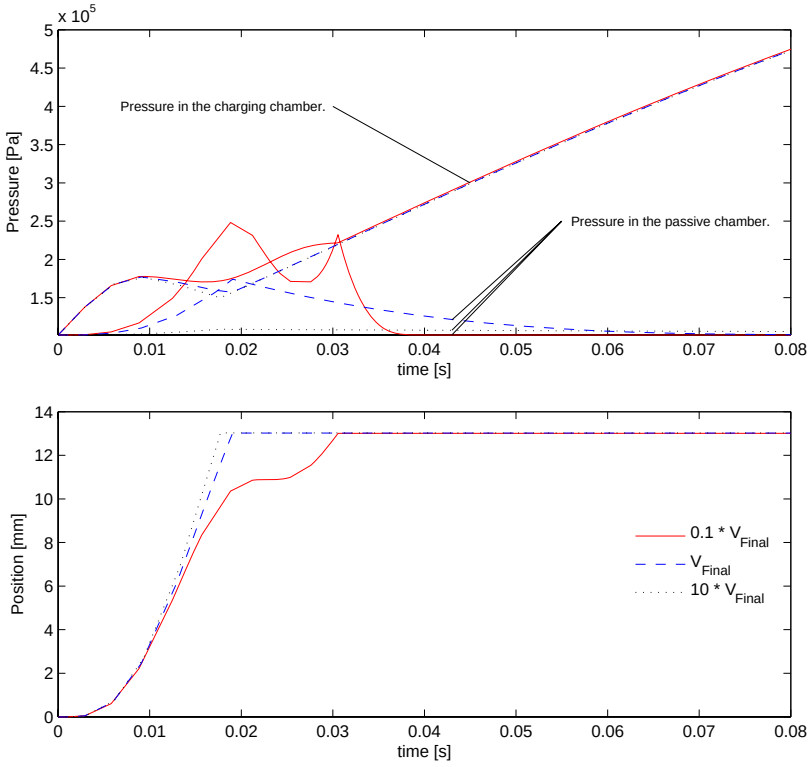

Figure 5.5. Effects of small and large final volumes.

5.4 Air inlet holes

In theory, the size of the air inlet hole is proportional to the massflow according to (3.13) and (3.14). In the same section it is also concluded that this relationship is not accurate. However, it can be concluded that the massflow is highly dependent of the inlet hole size. There are two problems determining how the massflow depends on the inlet holes. Since there is no accurate model, the same approach used in previous sections, where the system model is used, is out of the question. The other problem is the pathway the air takes traveling to the chamber, there are many small areas inside the solenoid valve which are immeasurable. So even if the chamber inlet holes are considered for resizing to allow measurements for mass flow dependence, it can not be guaranteed that there is not a smaller area somewhere in the solenoid valve.

Due to the complicating circumstances the influence of the inlet holes are remaining to be investigated by future researchers.

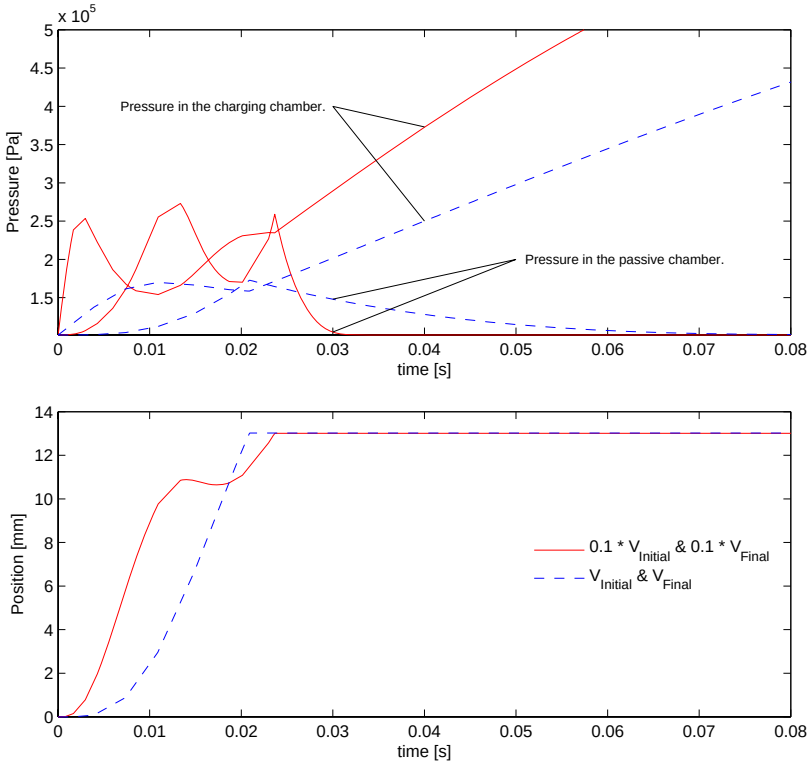

Figure 5.6. Effects of small final and initial volumes.

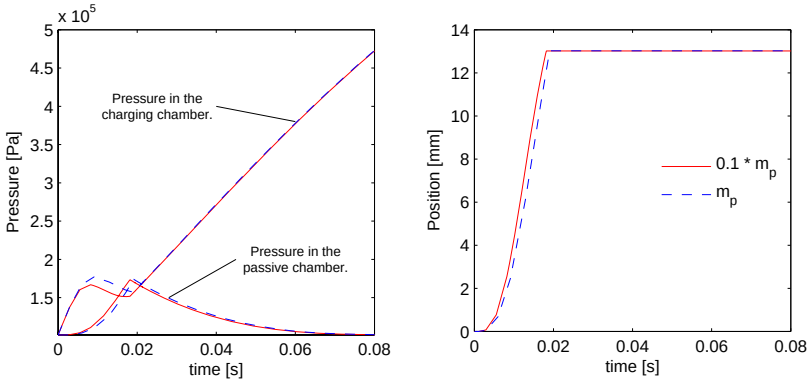

Figure 5.7. Fixed piston pneumatic force actuator with a lighter piston.

Chapter 6

Possible improvements

The system limitations discussed earlier are hard to deal with as they make it difficult to control this fast process. However, with the theory presented in previous chapters some ideas on how to improve the system are discussed. First the safety blow feature used in todays Opticruise setup is discussed and second, a approach using smaller final volumes, air cushion, is presented. Third, an outline for a feedback controller is briefly treated.

6.1 Safety blow

With todays OPC4 setup, filling of the chamber is not stopped directly when the piston reaches the end position. Filling continues 150 ms after OPC4 has recieved confirmation that the neutral gear is engadged or until the engine and gearbox RPM's are syncronized. A commonly seen side effect of this behaviour, seen in Figure 6.1, is that pressure in the neutral chamber is high when a new gear is to be engaged. This slows down the shifting process, since the neutral pressure has to be overcome. To find out how much time can be saved in every gear shift, numerous measurements has to be made and analyzed. However, brief analysis conducted on measurements from gearshifts in truck indicate that a time in the range of 50 - 100 ms can be saved on gearshifts when engaging a gear while pressure in the neutral chamber is high.

Another, more pleasing, side effect of shifts made during such conditions (high pressure in the neutral chamber) is the smoother movement of the gear. The high pressure (larger mass of air) in the neutral chamber acts as a cushion and deaccelerates the piston, reducing the effects of the impact between the piston and the chamber wall.

6.2 Air cushion

In 5.2.2 the benefits of small final chamber volumes are disscused. It is also mentioned that a rational choise of end volume, if possible, can replace the oil

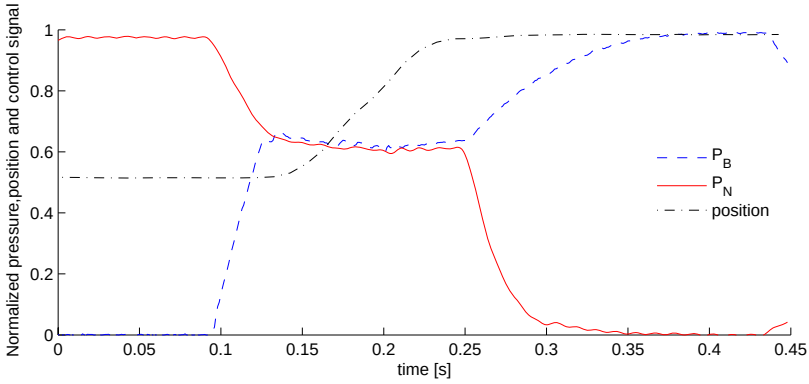

Figure 6.1. High pressure in the neutral chamber while engaging backward.

damper. The air cushion idea is simple, during piston movement (with the outlet holes eliminated) the influence of air in the passive chamber is being compressed with rising pressure according to:

$$\dot{P} = \alpha \frac{P}{V} \dot{V} \tag{6.1}$$

Especially, the pressure rise becomes extremly high when the chamber volume closes zero. Figure 6.2 show pressure versus volume in the fixed piston system using (6.1).

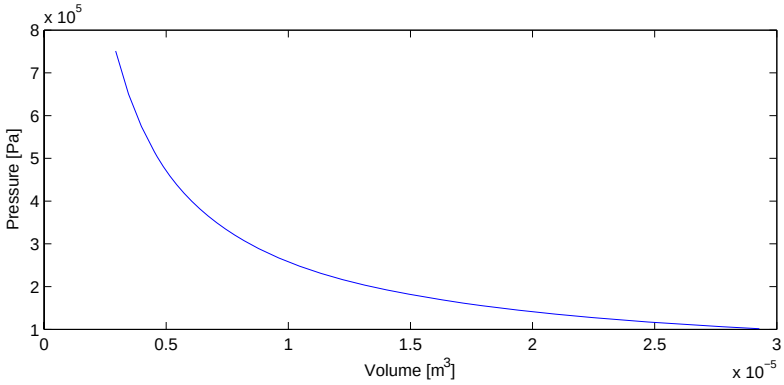

Figure 6.2. Pressure vs. volume when the chamber is reduced.

The trick is to have enough initial air so that when compressing, the chamber pressure becomes high enough to counteract the piston movement and have a damping effect before the piston reaches the chamber wall. However, with Figure 6.2 fresh in mind, one can conclude that enough initial air is equivalent with small

final volumes, since the pressure rise is extrem in this case. This is important, since it has been observed in 4.1 that the piston movement during the gearshifting process is not necesarilly smooth and continous allowing air to escape through the outlet hole. Figure 6.3 shows how this look during a gear shift in truck.

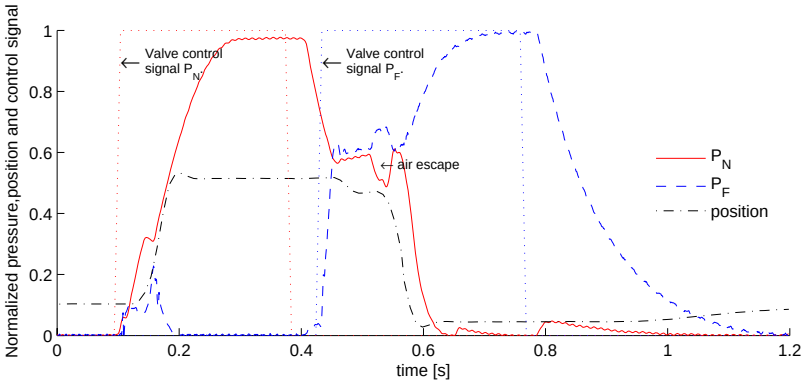

Figure 6.3. Air escape during gearshift.

Since the final volumes are the initial volumes for the reversed gearshift, some considerations must be taken into account when reducing these volumes. Todays system with, relatively, large final/initial volumes is constructed so that the pressure rise is distributed evenly in a fast way across the piston area. A reduction of these volumes would make it harder to produce the same effective path to distribute pressure over the piston area and can make the piston stuck. This is displayed in Figure 6.4.

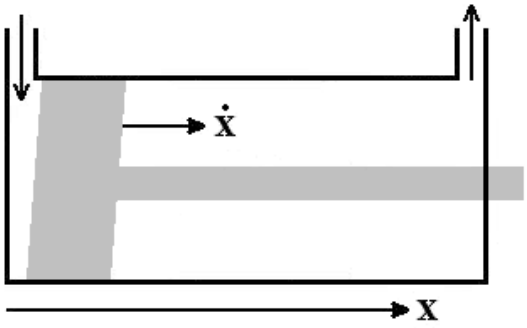

Figure 6.4. The piston is stuck due to uneven pressure over the piston area.

Another thing to be condcidered is the outlet holes. They have to be small enough so that no considerable amount of air is pressed out during chamber re-

duction but they still need to let out enough air so that the piston can reach the end position.

How to chose the outlet holes and construct a final volume so that the oil damper can be replaced, is left for future researchers to discover. Here it is merely concluded that this kind of solution is possible and interesting to look in to.

6.3 Feedback control

As concluded in 4.2.1 there is no time interval available for any kind of feedback control, since the process is over before the sensors, control unit (OPC4) and the valves have had time to react. As discussed in 2.2.4 it is possible to enhance the position sensor and the OPC4 so that a position measurement is given every 2-3 ms. With a position sensor this fast some sort of feedback air cushion might be possible. This of course requires fast valves and therfore the closing time for the solenoid valves has to be improved considerably.

If all of the above problems are eliminated it might be possible to use PMP to calculate the optimal feedback control law. Easier to implement is probably a feedback air cushion solution, Figure 6.5, where a short burst of air is pumped into the discharging chamber just before the end position is reached. Since the control signal $\boldsymbol{u}(t)$ is off bang bang (on/off) type a solution obtained from PMP is most likely very similar to the feedback air cushion, [8].

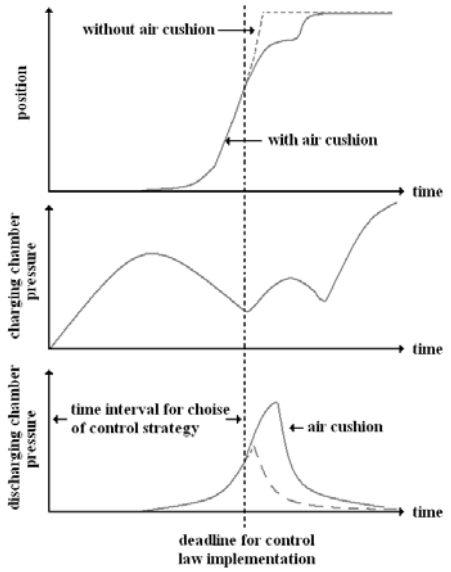

Figure 6.5. Outline for a feeback air cushion damper.

Chapter 7

Conclusions

A detailed physical system model of the length stroke in the Opticruise gear shifting system is developed. Validation against real data suggests that the model quality is sufficient for evaluating how hardware parameter changes affect system performance. This is very useful for the mechanical construction team since they can see how the system behaves with different parameters without building a prototype. This is of course time efficient and favorable from a cost reduction perspective.

As demonstrated in this thesis, the system is to fast for pneumatic feedback control using existing equipment. However, ideas for how to get around this problem, together with control strategies for the process are presented. It is also shown that a model predictive control strategy is problematic due to the high uncertainties using the model with the Opticruise unit installed in a truck.

The last approach, using small final volumes, is shown to have the best prospect of success since it is cheap, easy to produce, material-efficient and easy to implement.

Aims on how future work in this area can be continued is presented in Chapter 6.

Bibliography

[1] Al-Ibrahim A. M. and Otis D. R., *Transient Air Temperature and Pressure Measurements During the Charging and Discharging Processes of an actuating Pneumatic Cylinder*, Proceedings of the 45^{th} National Conference on Fluid Power, 1992.

[2] Bobrow J. E. and Lum K., *Adaptive, High Bandwidth Control of a Hydraulic Actuator*, Proceedings of the American Control Conference, Seattle, Washington, pp. 71-75, 1995.

[3] Bobrow J. E. and McDonell B. W., *Modeling, Identification, and Control of a Pneumatically Actuated, Force Controllable Robot*, IEEE Transactions on Robotics and Automation, Vol. 14, No.5, pp. 732-742, 1998.

[4] Evertsson N., *Personal communication*, Department of Powertrain Control Systems, NEP, Scania CV AB, 2007.

[5] He S. and Sepehri N., *Modeling and Prediction of Hydraulic Servo Actuators with Neural Networks*, Proceedings of the American Control Conference, pp. 3708-3712, 1999.

[6] Håkansson K. and Johansson M., *Modeling and Control of an Electro-Pneumatic Actuator System Using On/Off Valves*, Master thesis, LITH-ISY-EX–07/3971–SE, linköping, 2007.

[7] Insider secrets to hydraulics, *Compression and decompression of hydraulic fluid*, http://www.insidersecretstohydraulics.com/hydraulic-decompression.html, 2007-03-12.

[8] Jönsson U., Trygger C. and Ögren P., *Optimal Control - Lecture notes*, Department of Optimization and Systems Theory, KTH, 2006.

[9] Karlsson A., *Compressible flow - Solution Manual to Selected Problems*, 1998. Teaching material in fluid mechanichs, KTH.

[10] Kazerooni H., *Design and Analysis of Pneumatic Force Generators for Mobile Robotic Systems*, IEEE Transactions on Mechatronics, Vol. 10, No.4, pp. 411-418, 2005

[11] Ljung L. and Glad T., *Modellbygge och simulering*, Studentlitteratur, Lund, 2004

[12] Merritt H. E., *Hydraulic Control Systems*, John Wiley & Sons, Inc., 1967

[13] Niksefat N. and Sepehri N., *Designing Robust Force Control of Hydraulic Actuators Despite System and Environmental Uncertainties*, IEEE Control Systems Magazine, pp. 66-77 2001.

[14] Ning S., Otis D. R. and Beachley N. H., *Flow modeling for pneumatic cylinder actuation*. University of Wisconsin-Madison, Mechanical Engineering Department, Report No. ME-FP-901, 1990.

[15] Paul A. K., Mishra J. K. and Radke M. G., *Reduced Order Sliding Mode Control for Pneumatic Actuator*, IEEE Transactions on Control Systems Technology, Vol. 2, No. 3, pp. 271-276, 1994

[16] Rahman M. F., Cheung N. C. and Lim K. W., *Position Estimation in Solenoid Actuators*, IEEE Transactions on Industry Applications, Vol. 32, No. 3, pp. 552-559, 1996.

[17] Rao Z. and Bone G. M., *Modeling and Control of a Miniature Servo Pneumatic Actuator*, Proceedings of the 2006 IEEE International Conference on Robotics and Automation, pp. 1806-1811, 2006

[18] Richer E. and Hurmuzlu Y., *A High Performance Pneumatic Force Actuator System, Part 1 - Nonlinear Mathematical Model*. ASME journal of Dynamic Systems Measurement and Control, Vol. 122, No.3 pp. 416-425, 2000.

[19] *P900 Series - Premium Performance Strain Gauge*, Schaevitz, Datasheet, www.schaevitz.com, 2007.

[20] Shearer J. L., *Study of Pneumatic Processes in the Continuous Control of Motion With Compressed Air - I*, Transactions of the ASME, pp. 233-242, Feb., 1956.

[21] Song-Min W., Takashi M. and Mont H., *Electromagnetic Field Analysis and Dinamic Simulation of a Two-Valve Solenoid Actuator*, IEEE Transactions on Magnetics, Vol. 29, No. 2, pp. 1741-1746, 1993.

[22] *RLP - industriella, linjära Lägesgivare 0-600mm*, Swema, Datasheet, www.swema.se/Givare/frameGivare.html, 2007-02-15.

[23] Tan H.-S. and Bradshaw T., *Model identification of an automotive hydraulic active suspension system*, Proceedings of the American Control Conference, pp. 2920-2924, 1997.

[24] Topcu E. E., Yüksel İ. and Kamis Z., *Development of electro-pneumatic fast switching valve and investigation of its characteristics*, Mechatronics, Vol. 16, No. 6, pp. 365-378, 2006.

[25] Wu G., Sepehri N. and Ziaei K., *Design of a hydraulic force control system using a generalised predictive control algorithm*, IEE Proc.- Control Theory Appl., Vol. 145, No. 5, pp. 428-436, 1998.

[26] Yun J. S. and Cho H. S., *Application of an Adaptive Model Following Control Technique to a Hydraulic Servo System Subjected to Unknown Disturbances.* ASME journal of Dynamic Systems Measurement and Control, Vol. 113, No.3 pp. 479-486, 1991.